Journal Pre-proof

Hybrid Shunt Active Filter Based Amalgamated Controller Utilized for Power Quality Improvement with Harmonic Mitigation in Smart Grid System

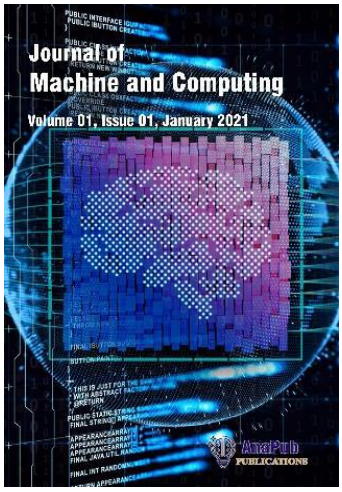

Omar A AlKawak, Hadi Saghafi, Ali A Abdullah Albakry, Bahador Fani and Majid Delshad

DOI: 10.53759/7669/jmc202505188

Reference: JMC202505188

Journal: Journal of Machine and Computing.

Received 23 April 2025

Revised from 02 June 2025

Accepted 04 August 2025

Please cite this article as: Omar A AlKawak, Hadi Saghafi, Ali A Abdullah Albakry, Bahador Fani and Majid Delshad, "Hybrid Shunt Active Filter Based Amalgamated Controller Utilized for Power Quality Improvement with Harmonic Mitigation in Smart Grid System", Journal of Machine and Computing. (2025). Doi: https:// doi.org/10.53759/7669/jmc202505188.

AnaPub PUBLICATIONS

Hybrid Shunt Active Filter Based Amalgamated Controller utilized for Power Quality Improvement with Harmonic Mitigation in Smart Grid system

*Omar A. AlKawak[1], Hadi Saghafi[*1], Ali A. Abdullah Albakry[2], Bahador Fani[1], Majid Delshad[1]*

[1] Department of Electrical Engineering, Isfahan (Khorasgan) Branch, Islamic Azad University, Isfahan, Iran

[2] Al-Furat Al-Awsat Technical University, Al-Musayyib Technical College, Electrical Engineering Techniques, Babil, Iraq

o0maar.g@gmail.com, h.saghafi@khuisf.ac.ir, draalia@gmail.com, b.fani@khuisf.ac.ir, delshad@khuisf.ac.ir

Corresponding author: h.saghafi@khuisf.ac.ir

Abstract

Earlier difficulties in reducing harmonics involved managing the unpredictable and varying characteristics of Renewable Energy Sources (RES), resonance problems with passive filters, the intricate design and expensive nature of active filters, and the shortcomings of traditional controllers such as PI controllers, which face difficulties with instant adjustments and accurate calibration in changing power networks. This research proposes an intelligent approach for an optimal controller designed for harmonic suppression to maintain Power Quality (PQ) in Renewable Energy Systems (RES) through the use of a distribution network featuring a hybrid shunt active filter (HSAF). The proposed intelligent technique merges the functionality of the Multi-Strategy Fennec Fox Algorithm (MSFA) with a fractional-order Proportional Integral Derivative (FOPID) controller. In this approach, the MSFA optimizes the basic and harmonic loop settings of the hybrid shunt active filter, including the DC voltage and terminal voltage parameters. This information set is created through modifications in RES characteristics and fluctuations in both linear and non-linear loads, which are all controlled by an error minimization objective function. The MSFA creates ideal control commands by accurately forecasting the necessary parameters through this comprehensive information set. This method enhances system precision by guaranteeing reduced complexity for harmonic reduction during PQ events. The suggested model is put into practice using the MATLAB/Simulink environment, and its effectiveness is assessed in comparison to current techniques. When harmonic correction is applied to the load side owing to harmonic sources, the load voltages' magnitude is balanced and

equal to one p.u. The total harmonic distortion (THD) of the load voltages and currents is kept at 0.81%.

Keywords: *Dynamic power systems, Distribution system, Harmonic loop parameters, Hybrid shunt active filter, Terminal voltage, DC voltage*

1. Introduction

Harmonic mitigation is essential in distribution systems that are based on Renewable Energy Systems (RES) [1]. Nonetheless, a number of noteworthy Power Quality (PQ) problems are deemed prominent, including noise, flicker, transients, swells, sags, harmonics, and notching [2, 3]. Loose connections and network overloading can cause voltage changes. A sinusoidal voltage source produces non-sinusoidal currents due to non-linear loads, which results in harmonics in the voltage and current signals [4, 5]. These harmonics cause damage to the equipment in the distribution system, such as overheating of the transformer and rotating machine, malfunctioning of the protective devices, nonlinear loading of the bus bars, failures of the capacitor bank, and more [6]. To address these equipment issues caused by harmonics, utilities and industrial users often employ harmonic compensation methods. The selection of harmonic filtering systems in industrial power systems depends largely on the severity of harmonic contamination [7].

Many loads, including electric arc furnaces, capacitor switching, DC converters, inverters, static VAR compensators, switch-mode power supplies, AC or DC motor drives, and lightning strikes, are the source of harmonics [8]. These disturbances often lead to equipment malfunctions, reduced lifetimes, and failures. Researchers have employed various technologies for harmonic mitigation; including recursive least squares (RLS) and differential evolution (DE) algorithms [9]. RLS is criticised for being unstable and complex, even though it computes the error value between the desired signal and the filter output. Although it can take a while, DE is preferred for continual function optimisation. These techniques are useful in reducing Power Quality (PQ) disturbances such as harmonics, but they become more difficult because more samples are required [10]. Overcoming these challenges requires advanced technologies for harmonic mitigation.

1.1. Review Literature

Numerous studies that focused on reducing harmonic resonance in distribution systems using various techniques and viewpoints have already been outlined in the literature [11–20].

Reguieg, Z et al. [21] have performed to maintain high-quality power in interconnected renewable energy systems. The focus was on solar photovoltaic and wind energy sources that connect to the existing power grid using alternating current. Solar and wind systems use power

electronics to interface with the grid. These devices, while necessary, can introduce distortions in the voltage waveform (harmonics). This study recognizes this and proposes using a Series Active Power Filter (SAPF) to reduce these harmonics.

Mukherjee, S et al. [22] have illustrated the simulation model of a grid-connected photovoltaic (PV) system. The model was used to analyze the impact of harmonics on the system when nonlinear loads are present. The simulation demonstrates the creation of different odd-order harmonics that may harm the system's overall functionality.

K.A.M. and Abdullah, N [23] have explained how an active-passive hybrid harmonic power filter can be used to eliminate harmonic distortion in three-phase electrical networks. The effectiveness of this filtering system was evaluated through practical laboratory experiments using a 240V setup along with MATLAB modeling. Non-linear loads were modeled to replicate actual operating conditions, incorporating an uncontrolled rectifier paired with a series-connected RLC load. Selected results were presented to demonstrate the filter's capability in reducing harmonic interference.

Li, S et al. [24] have introduced a new method called Active Filter Tuning (AFT). AFT aims to provide a unified strategy for tuning and assessing the stability of two harmonic impedance reshaping (HIR) methods: current-controlled and voltage-controlled. AFT achieves this by introducing a "coordination factor."

Amini, B and colleagues have described a technique for enhancing power quality within electrical networks. Their work outlines the fundamental concepts underlying SAPF architecture and presents an improved control strategy. The description incorporates suitable system modeling to facilitate comprehension. To accomplish superior current regulation, the study suggests an innovative method: a Proportional-Resonant (PR) controller optimized through a Genetic Algorithm (GA). The PR controller proves well-suited for SAPF applications because of its capability to accurately detect and react to harmonic currents. This results in quicker and more precise operation when identifying disturbances and producing compensating waveforms.

Govind, A., et al. shown a systematic technique to improving power quality using SAPF. The strategy contains a number of critical components: Neural network control improves SAPF switching control, especially under dynamic and nonlinear load settings. It operates as a "smart" controller, capable of adapting to changing situations. The Proportional-Integral (PI) controller maintains a constant and controlled voltage at the DC connection, a critical component of the SAPF.

Rezapour, H et al. have estimated a novel method to simultaneously improve power quality, reduce losses, and maintain voltage stability in distribution networks. It achieves this by strategically placing two key components: By combining these elements, the proposed method offers a more comprehensive and effective way to optimize power distribution networks, leading to cleaner power, reduced energy waste, and improved voltage regulation.

Karbasforooshan, M.S. and Monfared, M have elucidated a new approach to designing power filters that prioritizes simplicity and effectiveness. The filter's structure and its ability to filter out unwanted signals (filtering characteristics) were modeled in a clear and understandable way. This allows engineers to easily predict the filter's performance. A proportional controller tracks the reference current effectively. This controller has sufficient bandwidth for fast response and a built-in stability margin to prevent unwanted oscillations.

P. Daramukkala et al.'s novel strategy addresses PQ problems in electrical distribution networks. Enhancing the quality of current that the utility provides to end users was the main goal. The method that is being discussed uses an exponential functional link network (EFLN) in conjunction with a Nonlinear Adaptive Filtering (NAF) method to operate a Shunt Hybrid Active Power Filter (SHAPF).

Gupta, U.K et al. have estimated a growing challenge in the Internet of Things (IoT) world: protecting sensitive devices from power quality issues caused by smart devices themselves. Many smart devices contain non-linear loads that generate unwanted distortions in the power supply (harmonics). These harmonics can disrupt the operation of other devices, especially those with sensitive sensors. To address this, the study presents a novel technique using a Takagi-Sugeno (TS) Neuro-Fuzzy (TS-ANFIS) system to supervise a SAPF.

1.2. Research Motivation

Harmonic mitigation serves as a cornerstone for preserving power quality and system stability in electrical networks, particularly when integrating Renewable Energy Sources (RES). Hybrid Shunt Active Power Filters (HSAPFs) emerge as crucial components in tackling this issue by merging passive and active filtering approaches to eliminate harmonic distortions efficiently. The growing implementation of RES like solar and wind energy brings intermittent and non-linear behavior to the electrical grid, causing substantial harmonic production. These harmonics can compromise power quality, trigger equipment malfunctions, and elevate total system losses.

The core drive behind research in this domain centers on creating effective and adaptable filtering mechanisms that can handle the changing characteristics of power systems integrated

with RES. Traditional methods such as passive filters provide economic advantages but face challenges including resonance problems and static compensation capabilities. Active Power Filters (APFs) deliver dynamic compensation yet involve complexity and high costs. Hybrid filtering systems seek to combine the advantages of both passive and active approaches; nevertheless, their success depends on advanced control methodologies.

Standard controllers like Proportional-Integral (PI) controllers see widespread use but face difficulties with the non-linear and time-dependent features of RES. These controllers typically demand accurate calibration and might fail to react swiftly to abrupt system variations, resulting in less-than-ideal performance. To overcome these obstacles, there exists an evident requirement for smart controllers that can adapt in real-time to changing conditions within RES-integrated power networks. These advanced controllers can guarantee dependable and effective harmonic reduction, thus improving overall power quality and system dependability.

1.3. Research Objectives and Contributions

This research introduces a smart hybrid method for reducing harmonics in distribution systems that combine hybrid shunt active power filters with renewable energy sources. The primary goal focuses on enhancing power quality by effectively minimizing harmonic distortion. The proposed technique utilizes MSFA to generate an optimal dataset that emphasizes key fundamental and harmonic loop characteristics, including DC and terminal voltage measurements. MSFA then uses this generated dataset to fine-tune these control signals, enabling effective harmonic suppression. The section that follows goes into the suggested approach's thorough methodology. The rest of the document is organized as follows: The hybrid shunt active power filters linked to RES for harmonic mitigation are described as a system in Section 2. The suggested strategy for harmonic mitigation is described in Section 3. The simulation findings and conclusions are presented in Sections 4 and 5, respectively. Every segment adds to the understanding of how the intelligent hybrid approach works and how to apply it to enhance power quality in distribution systems with RES integration by mitigating harmonics.

2. System Description of the Hybrid Shunt Active Power Filter Connected RES

Figure 1 shows the HSAF combined with RES system configuration. The PV array linked to the boost DC-DC converter at the beginning of the conversion chain is shown in this image. By attaining optimum power extraction under steady-state conditions through impedance matching made possible by the static converter, the MSFA-based controller guarantees optimal operation.

In the next phase of the system, an inductive filter is used to link three-phase, two-level inverters to the grid. As HSAFs, these inverters balance reactive power requirements as well as harmonic distortions brought on by non-linear loads in the AC mains. The FOPID controller is employed as the control strategy for the DC/AC inverter, facilitating effective power sharing between the PV array and the grid under varying irradiance levels. This system configuration highlights the integration of RES, particularly PV arrays, with advanced control techniques aimed at optimizing power extraction and mitigating harmonics to improve overall power quality in distribution systems.

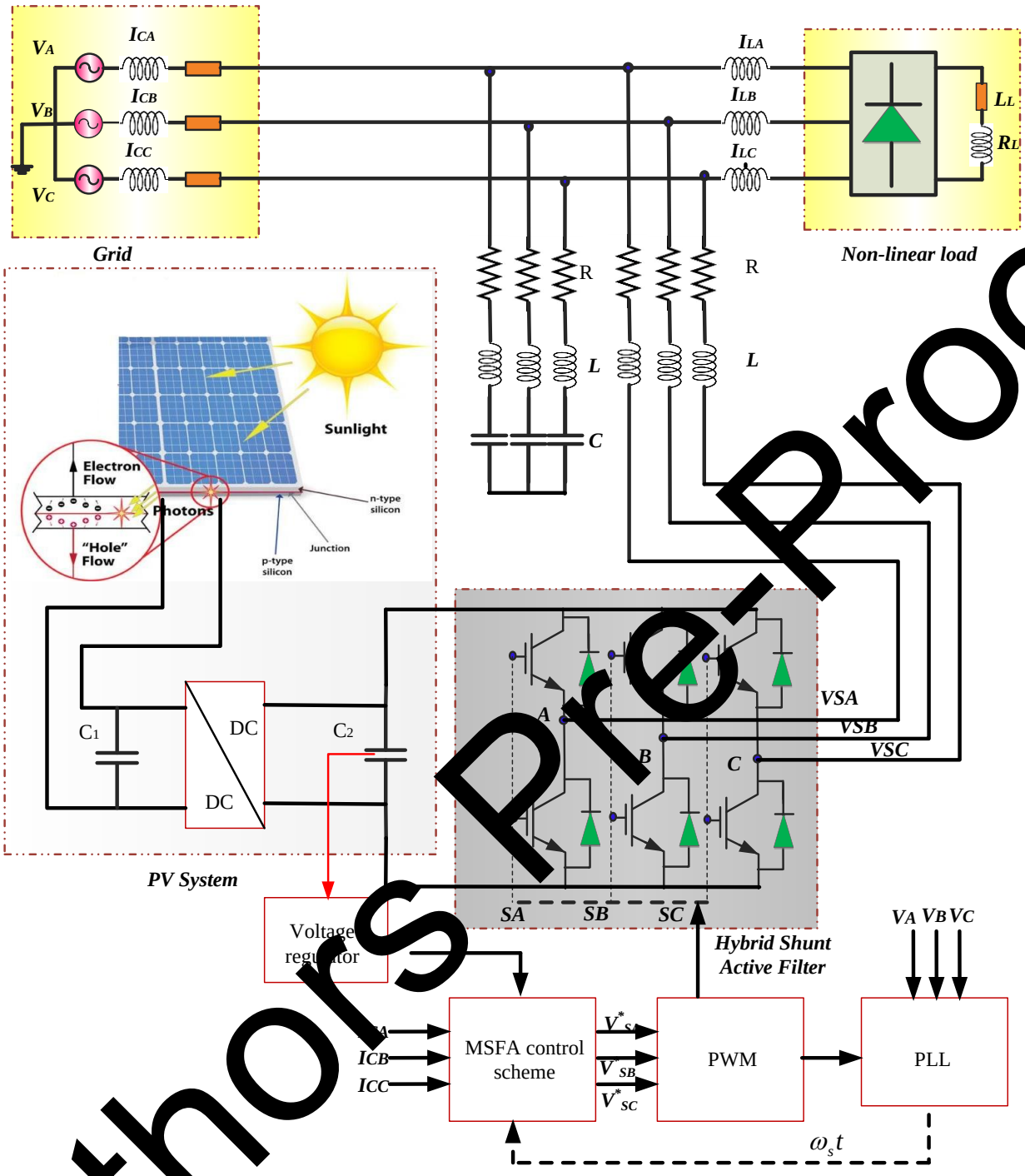

Figure 1. System Overview of the Hybrid Shunt Active Power Filter under Proposal for Distribution System

2.1. Control approaches

The main goal of the proposed control strategies is to achieve these targets through effective management of the various static converters involved, especially those connected to the photovoltaic and electrical grid systems. These approaches have been completely developed and refined for each component before being applied and validated in actual operating environments.

The focus centers on guaranteeing reliable and optimal control of static converters, which serve as essential elements in systems that combine solar panel arrays with grid infrastructure. Through the enhancement of control techniques for these converters, the study seeks to improve total system functionality, including optimizing energy harvest from solar installations, reducing electrical disturbances, and facilitating seamless grid integration.

Before implementation in real-world applications, comprehensive simulation studies and potential prototype evaluations are usually performed to confirm the success and dependability of the suggested control methods. This thorough validation process guarantees that the techniques are sufficiently durable to manage the changing operational circumstances and fluctuations found in actual renewable energy source-integrated power distribution networks.

2.1.1. Mathematical Formulation of PV side control

The photovoltaic system consists of multiple solar cells arranged in series and configured as an array to deliver the required voltage and current for microgrids and electrical loads. These solar cells exhibit nonlinear voltage-current behavior that responds to solar radiation levels, which can be described in the following manner:

Solar irradiance fluctuates during daily cycles and varies with changing weather patterns, causing the performance characteristics of the PV system to shift correspondingly. When irradiance drops to lower levels, the photovoltaic cells generate reduced current and voltage outputs below their specified ratings. Conversely, when irradiance intensifies, both current and voltage outputs climb toward the array's optimal power point (MPP).

Due to the inherent properties of semiconductor materials within solar cells, the voltage-current relationship in PV systems follows a nonlinear pattern. This nonlinear behavior is commonly represented through the current-voltage (I-V) characteristic curve, which demonstrates how current output grows alongside increasing voltage until it peaks at the MPP. Past this optimal point, any additional voltage increases lead to declining current production.. Practically, the nonlinear properties of the PV generator require complex control techniques, including Maximum Power Point Tracking (MPPT), to guarantee that the system runs at or close to its MPP in a variety of solar conditions. This optimization is crucial for maximizing energy extraction from the PV array and ensuring efficient operation within the microgrid and load requirements.

$$V_g = \frac{1}{A_g} \ln\left[\frac{GI_{pvg} - I_g + I_{og}}{I_{og}}\right] - I_g R_{sg} \quad (1)$$

where, I_g and v_g denotes generated current and voltage, $I_{og} = I_o \times N_p$ denotes reverse saturation current. $A_g = Z/N_s$ represents the constant of the PV generator, $Z = q/(\xi \times K \times T)$ denotes constant, ξ denotes completion factor, K denotes Boltzmann constant, T denotes absolute temperature and q denotes charge of the electron. $R_{sg} = R_s \times (N_s/N_p)$ represents the series resistance, R_s denotes series resistance, N_s and N_p denotes series and parallel connected cell. $I_{pvg} = I_{pv} \times N_p$ denotes PV generated current and I_{pv} denotes PV current per cell. G is the solar insolation and $G = 1000W/m^2$ has 1.0 per unit. At certain value of G, the PV module output power is maximum at unique point. This point is termed the Maximum Power Point (MPP) and its position is located by deciding the equivalent voltage v_{gm} and current I_{gm}. The dynamic model of the buck-boost DC-DC converter can be composed as

$$\frac{dI_l}{dt} = -\frac{V_s}{L_s} - \frac{(v/V_s)}{L_s} D \tag{2}$$

$$\frac{dV_{dc}}{dt} = \frac{I_l}{C_s} - \frac{V_{dc}}{C_s} - \frac{I_l}{C_s} D \tag{3}$$

where, L_s and C_s denotes electrical parameters, I_l denotes current across the inductor and D denotes duty ratio of the buck-boost converter.

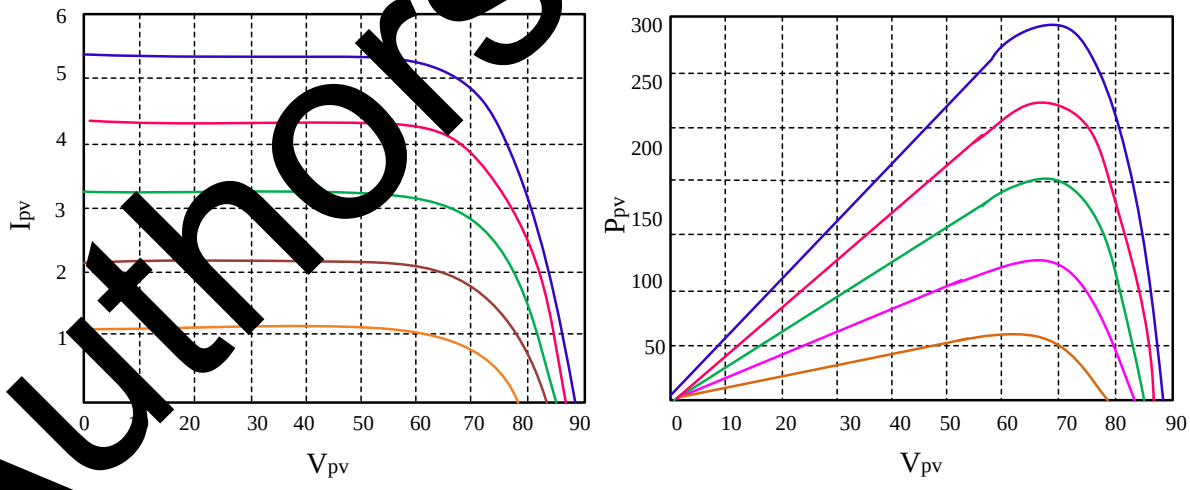

Figure 2: I-V characteristic (a), P-V characteristic (b) under different irradiance conditions.

The I-V characteristics of the solar PV array at different levels of irradiation are depicted in Figure 2. The maximum power point (MPP) at which the photovoltaic array may produce its

highest power output and hence maximise the utilisation of available solar energy is represented by the operation point at the knee of the curve, as shown in Figure 2(b). The suggested-based, quick, and accurate Maximum Power Point Tracking (MPPT) technique is used to do this; it is especially well suited for PV systems. This method, known for its local optimization approach, is effective under typical radiation patterns, being robust, integrated, straightforward, and not reliant on complex system modeling. A FOPID controller is used in this system to effectively distribute power demand between the grid and the PV array. In the following section of this paper, the mathematical formulations of the FOPID control strategy and the hybrid shunt active power filter are presented along with their respective roles in RES-integrated distribution systems power quality enhancement and system performance optimisation.

2.1.2. Mathematical Formulation of FOPID Controller

The suggested technique incorporates a Fractional Order Proportional Integral Derivative (FOPID) controller, which is schematically shown in Figure 3. The controller is designed to adapt its reaction in order to meet predetermined performance targets. To address computational complexity and implementation challenges, the initially higher-order FOPID configuration is frequently simplified to a lower-order representation. This simplification strategy ensures that the controller maintains its effectiveness while improving practical applicability. The closed-loop behavior of the reduced-order FOPID controller efficiently captures the dynamic response characteristics originally intended by the higher-order design.

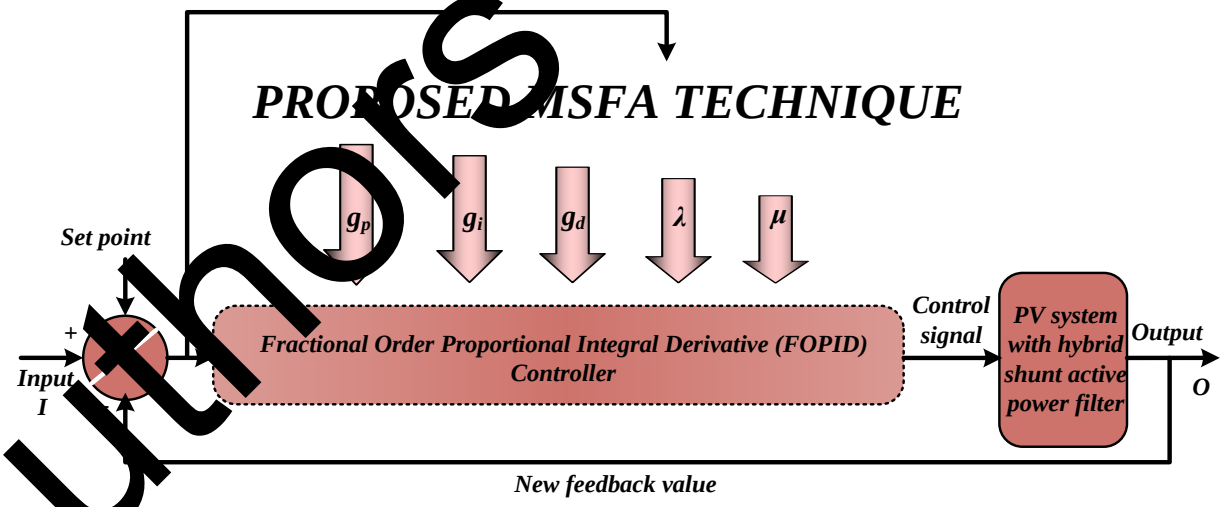

Figure 3: Schematic of FOPID controller with proposed technique

Modelling of g_P

The relationship is obtained by taking the derivative of error 'e' with respect to the proportional gain (g_p):

$$e = \left[\frac{gg_p + gg_i \times \frac{1}{s^{\lambda}} + gg_d s^{\mu}}{Ts + 1 + g_p + gg_d s^{\mu} + gg_i \times \frac{1}{s^{\lambda}}} - \frac{g_m}{T_m s + 1} \right] \tag{4}$$

$$\frac{\partial e}{\partial g_P} = \left[\begin{array}{l} g\left(Ts + gg_P + gg_D s^{\mu} + gg_I \times \frac{1}{s^{\lambda}} + 1 \right)^{-1} - \\ g\ \left(gg_p + gg_i \times \frac{1}{s^{\lambda}} + gg_d s^{\mu} \right)\left(\left(Ts + gg_p + gg_d s^{\mu} + gg_i \times \frac{1}{s^{\lambda}} + 1 \right)^2 \right)^{-1} \end{array} \right] \eta_c \tag{5}$$

Then the formulation is simplified in the following,

$$\frac{\partial e}{\partial g_p} = \left[g^2 e\left(Ts + gg_p + gg_I \times \frac{1}{s^{\lambda}} + gg_d s^{\mu} + 1 \right)^{-1} \right] x \tag{6}$$

Modelling of g_i

Deriving '*e*' respect to the integral gain (g_i) is given in the following:

$$\frac{\partial e}{\partial g_i} = \frac{1}{s^{\lambda}} \left[\begin{array}{l} k\left(Ts + gg_p + gg_i s^{\mu} + gg_d \times \frac{1}{s^{\lambda}} + 1 \right)^{-1} \\ - g\ \left(gg_p + gg_i \times \frac{1}{s^{\lambda}} + gg_d s^{\mu} \right)\left(\left(Ts + gg_p + gg_i s^{\mu} + gg_d \times \frac{1}{s^{\lambda}} + 1 \right)^2 \right)^{-1} \end{array} \right] \eta_c \tag{7}$$

This equation is also be expressed as:

$$\frac{\partial e}{\partial g_i} = \frac{1}{s^{\lambda}} \left[g(Ts+1)\left(\left(Ts + gg_p + gg_i \times \frac{1}{s^{\lambda}} + gg_d s^{\mu} + 1 \right)\left(gg_P + gg_i \times \frac{1}{s^{\lambda}} + gg_d s^{\mu} \right) \right)^{-1} \right] x \tag{8}$$

Modelling of g_d

The following formulation is obtained by deriving e with regard to the derivative gain (g_d).

$$\frac{\partial e}{\partial g_d} = \left[gs^{\mu}\left(Ts + gg_p + gg_i \times \frac{1}{s^{\lambda}} + gg_d s^{\mu} + 1 \right)^{-1} - \frac{gs^{\mu}\left(gg_p + gg_i \times \frac{1}{s^{\lambda}} + gg_d s^{\mu} \right)}{\left(Ts + gg_p + gg_i \times \frac{1}{s^{\lambda}} + gg_d s^{\mu} + 1 \right)^2} \right] \eta_c \tag{9}$$

The above equation is also written as,

$$\frac{\partial e}{\partial g_d} = \left[\frac{gs^{\mu}(Ts+1)}{\left(Ts + gg_p + gg_i \times \frac{1}{s^{\lambda}} + gg_d s^{\mu} + 1 \right)\left(gg_p + gg_i \times \frac{1}{s^{\lambda}} + gg_d s^{\mu} \right)} \right] x \tag{10}$$

Modelling of λ

The following formula is used to get 'e' with regard to the fractional order integral (λ):

$$\frac{\partial e}{\partial \lambda} = \frac{gg_i \ln(s)}{s^{\lambda}} \left[\frac{\left(gg_p + gg_i \frac{1}{s^{\lambda}} + gg_d s^{\mu} \right)}{\left(Ts + gg_p + gg_i \times \frac{1}{s^{\lambda}} + gg_d s^{\mu} + 1 \right)^2} - \frac{1}{\left(Ts + gg_p + gg_i \times \frac{1}{s^{\lambda}} + gg_d s^{\mu} + 1 \right)} \right] \eta_c \quad (11)$$

The above equation is written as,

$$\frac{\partial e}{\partial \lambda} = \frac{gg_i \ln(s)}{s^{\lambda}} \left[\frac{-(Ts+1)}{\left(Ts + gg_p + gg_i \times \frac{1}{s^{\lambda}} + gg_d s^{\mu} + 1 \right)\left(gg_p + gg_i \times \frac{1}{s^{\lambda}} + gg_d s^{\mu} \right)} \right] x \quad (12)$$

Modelling of μ

The formulation is represented as follows, which is the derivation connected to 'e' with regard to the fractional-order derivative (μ).

$$\frac{\partial e}{\partial \mu} = \left[\frac{\left(gg_d s^{\mu} \ln(s) \right)}{\left(Ts + gg_p + gg_i \times \frac{1}{s^{\lambda}} + gg_d s^{\mu} + 1 \right)} - \frac{gg_d s^{\mu} \ln(s) \left(gg_p + gg_i \times \frac{1}{s^{\lambda}} + gg_d s^{\mu} \right)}{\left(Ts + gg_p + gg_i \times \frac{1}{s^{\lambda}} + gg_d s^{\mu} + 1 \right)} \right] \eta_c \quad (13)$$

The above equation is also written as,

$$\frac{\partial e}{\partial \mu} = \left[\frac{gg_d s^{\mu} \ln(s)(Ts+1)}{\left(Ts + gg_p + gg_i \times \frac{1}{s^{\lambda}} + gg_d s^{\mu} + 1 \right)\left(gg_p + gg_i \times \frac{1}{s^{\lambda}} + gg_d s^{\mu} \right)} \right] x \quad (14)$$

3. Harmonics Mitigation using Hybrid Approach

In harmonic mitigation, the FOPID controller demonstrates superior performance compared to a traditional PID controller due to its high stability, minimal peak overshoot, and reduced settling time. Managing harmonic distortions is critical in power systems where both linear and nonlinear loads contribute to voltage fluctuations generated by inverters. To mitigate THD in output

voltage and ensure high power quality, precise control of output parameters is essential. The proposed MSFA-based MPPT controller addresses these challenges effectively. The MSFA improves dataset accuracy by optimising principal and harmonic loop parameters within the hybrid shunt active filter, such as DC voltage and terminal voltage. It generates optimal control signals based on this data, effectively reducing THD through precise switching control pulses. The MSFA algorithm controls error voltage, comparing actual load voltage with reference sinusoidal voltage, ensuring accurate switching pulses for improved power quality. Detailed steps of the MSFA, including population initialization, Dynamic Convergence Factor (DCF), Adaptive Inertia Weights (AIW), Levy Flight Mechanism Strategy (LFMS), Evolutionary Population Dynamics (EPD), and termination process, illustrate its effectiveness as an optimization algorithm compared to existing methods. This approach is crucial for advancing harmonic mitigation strategies in modern power systems.

Step -1

Every fennec fox in the population is a representative of a search population member in the population-based metaheuristic algorithm known as FFO. An fennec fox may be represented mathematically as a vector, and the population matrix is made up of all of these vectors combined.

$$\begin{bmatrix} Y_{1,1} & \cdots & Y_{1,j} & \cdots & Y_{1,n} \\ Y_{2,1} & \cdots & Y_{2,j} & \cdots & Y_{2,n} \\ \cdots & \cdots & \cdots & \cdots & \cdots \\ \vdots & \vdots & \vdots & \vdots & \vdots \\ Y_{N-1,1} & \cdots & Y_{N-1,j} & \cdots & Y_{N-1,n} \\ Y_{N,1} & \cdots & Y_{N,j} & \cdots & Y_{N,n} \end{bmatrix} \tag{15}$$

where, N as count of prey population, n as dimensions.

$$Y_1(t) = Y_M(t) - E \cdot \left| Y_M(t) - rl \cdot \Pr ey(t) \right| \tag{16}$$

$$Y_2(t) = Y_{FM}(t) - E \cdot \left| Y_{FM}(t) - rl \cdot \Pr ey(t) \right| \tag{17}$$

where, t as current iteration, $Y_M(t)$, $Y_{FM}(t)$ as positions of fennec fox, and $\Pr ey(t)$ as position vector of prey. $Y_1(t)$ and $Y_2(t)$ as updated positions of fennec fox. E as terminating energy of prey. Thus, it is expressed below,

$$E = E \cdot E_0 \tag{18}$$

$$E_1 = c_1 \cdot (1 - (t/T)) \tag{19}$$

where, E_0 as random num in [-1,1] by specifying the initial energy of prey, T as maximal count of iterations, $E = E \cdot E_0$ denoted as the default constant set to 1.5 and E_1 denoted as the preys decreasing energy.

Step-2

In the MSFA, $\overline{A}$ is employed to modify the algorithm's abilities in local and global search. The fluctuation range of convergence factor and it shows that, if the 'm' and 'n' values are 2 and 6 that experience the better results. The $\overline{A}$ value is greatly influenced by the factor of convergence 'a'. A larger 'a' promotes search, enhancing the capacity to escape local optima. Conversely, a smaller 'a' strengthens local search and speeds up convergence. Adaptively adjusting 'a' aids in balancing the algorithm's global and local search capabilities. The equation for 'a' is given in equation (20):

$$a(t) = \frac{m}{e^{n\frac{t}{T_{\max}}}} \tag{20}$$

where, $'m','n',T_{\max},'t'$ represents optional parameters, maximum iterations, current number of iterations respectively.

Step-3

The weight of inertia is a crucial parameter in the cat swarm approach, holds significant importance in optimizing the objective function. A higher inertia weight enhances the search ability, enabling exploration across a wide region. MSFA presents the approach; to modify the weight depends on the iteration numbers by adaptation approach. The mathematical expression is given in equations (21-24):

$$w(k) = m \times \cos^n(\log(1 - e^{\frac{k}{T_{\max}}})) + 0.5 \tag{21}$$

The cat swarm position is expressed in following equation (3.39),

$$\vec{Y}(k+1) = w(k) \times \vec{Y}^*(k) - \vec{A}\vec{D} \tag{22}$$

$$\vec{Y}(k+1) = w(k) \times \vec{Y}_{rand}(k) - \vec{A}.|\vec{C}.\vec{Y}_{rand}(k) - \vec{Y}(k)| \tag{23}$$

$$\vec{Y}(k+1) = \vec{D}'.e^{bl}.\cos(2\Pi l) + w(k) \times \vec{Y}^*(k) \tag{24}$$

where, $\vec{Y}^{*}(k), \vec{A}, \vec{C}, \vec{D}, w(k)$ represents position vector with respect to 'k', vector coefficients, distance between the individuals, adaptive inertia weight respectively. Also $\vec{Y}_{rand}$,'l' represents random position vector, random number between [-1, 1] respectively.

Step-4

Many of the researchers discovered that numerous organisms favor employing the LFMS during hunting, especially in unpredictable conditions. Consequently, several heuristic algorithms have adopted this strategy, leading to improved performance in tackling randomized exploration challenges. Moreover, LFMS incorporates alternating frequency and rang exploration to evade getting trapped in local optima during the quest for optimal solutions across a broad spectrum. The mathematical expression of levy mechanism is given in equation (25-29)

$$L(s,\gamma,\mu)=\begin{cases}\sqrt{\dfrac{\gamma}{2\Pi}}\exp\left[-\dfrac{\gamma}{2(s-\mu)}\right]\dfrac{1}{(s-\mu)^{3/2}}, 0<\mu<s<\infty \\ 0, \quad otherwise\end{cases} \tag{25}$$

$$L(s,\gamma,\mu)\approx\sqrt{\frac{\gamma}{2\Pi}}\frac{1}{s^{3/2}} \tag{26}$$

$$L(s)=\frac{\alpha\beta\Gamma(\beta)\sin(\Pi\beta/2)}{\Pi|s|^{1+\beta}}, s\to\infty \tag{27}$$

$$s=\frac{u}{|v|^{1/\beta}} \tag{28}$$

$$\begin{cases}\sigma_u=\left\{\dfrac{\Gamma(1+\beta)\sin(\Pi\beta/2)}{\Gamma[(1+\beta)/2]\beta 2^{(\beta-1)/2}}\right\}^{\beta} \\ \sigma_v\end{cases}=1 \tag{29}$$

where, $L(s), \gamma, \mu, \Gamma, 'v'$ represents probability of moving steps, scale parameter, control variable, levy flight path, gamma function, random variables respectively. The algorithm updates the location of population based on the Lévy-flight mechanism while reducing the functional optimization obstacles. The expression of $Y_i(k+1)$ is given in equation (30),

$$Y_i(k+1)=w(k)\times Y_i(k)+(2r-1)*(Y_i(k)+r*s) \tag{30}$$

where, $'r', *$ represents random number between [0,1] and dot product between elements.

Step-5

The primary theoretical foundation of EPD is derived from self-organized criticality theory. According to this theory, the natural mutations occurring within species, without external

interference, can effectively address the inherent contradictions within populations. EPD is defined as the implementation of neglecting poorly individuals from the population. The formula for changing the poorer solution with the cat swarm location is given in equation (31),

$$Y_i(k+1) = \vec{Y}^{*}(k) + sign(r - 0.5) \times (ub - lb \cdot r + lb) \quad (31)$$

where $Y_i(k+1)$ denotes new position of multi-strategy cat swarm and sign values ranges are [-1,0,1].

Step-6

The initial approach aims to boost the middle of the population with every cycle, while the next method leverages the recent location of the whale as a potential person's location. Equation (31) modified in equation (32) as below:

$$Y_i(k+1) = \vec{Y}(k) + sign(r - 0.5) \times (ub - lb \cdot r + lb) \quad (32)$$

This mechanism proves highly beneficial for both exploration and overcoming local optimal stagnation. MSFA and its steps such as population initialization, DCF, AIW, LFMS, EPD, termination process is given in the Figure 4.

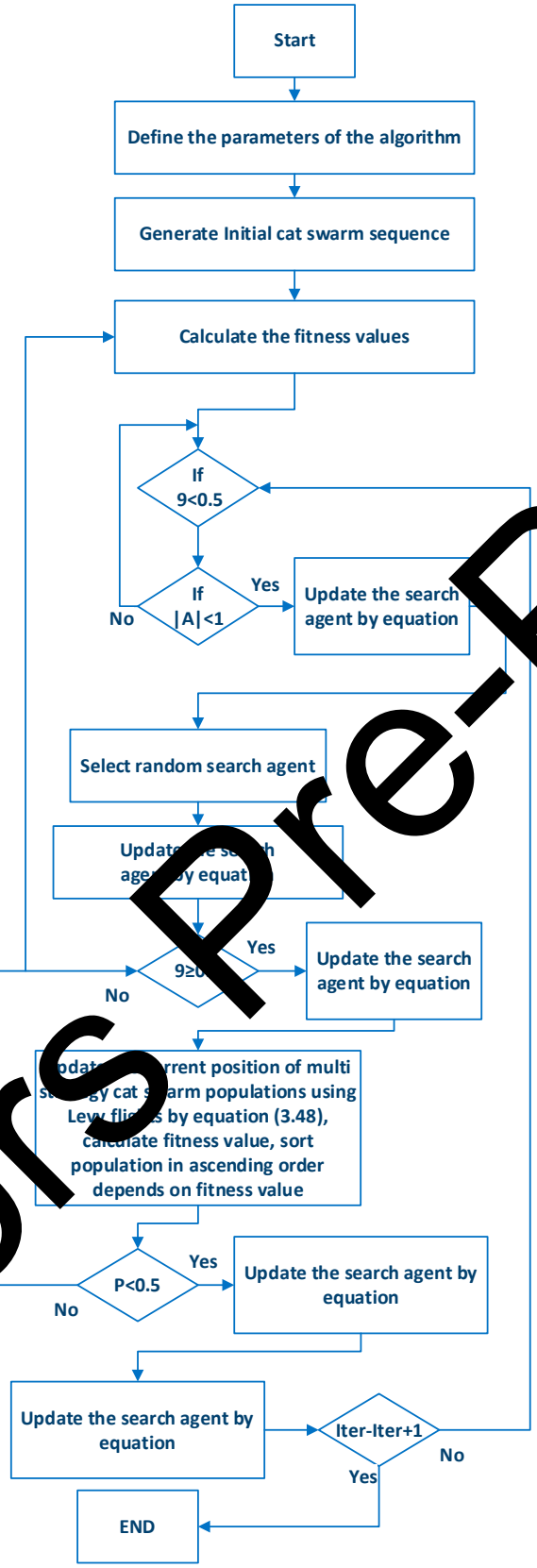

Figure 4: Layout for MSFA

4. Simulation Results and Discussions

In order to sustain PQ in RES-based distribution systems, this study presents an intelligent optimum controller. In the controller design, MSFA is used. The suggested method is simulated using the MATLAB/Simulink software. Thorough simulation evaluations encompassing various situations with different combinations of non-linear loads are used to assess the approach's efficacy.

(a) Grid harmonic current compensation caused by non-linear load

The system's operation in this scenario entails dynamic responses to different load circumstances and grid voltage disturbances. In order to provide the load with reference active and reactive powers at rated voltage and current, Mode A is first engaged from t = 0 to 0.1s. Then, a voltage sag of 0.4 p.u. initiates Modes B and C simultaneously from t = 0.1 to 0.2s. A voltage swell of 0.3 p.u. reactivates Modes B and C between t = 0.2 and 0.3s. Phases a, b, and c exhibit source voltage imbalances at magnitudes of 1.3 p.u., 0.7 p.u., and 1 p.u., respectively, as one moves to t = 0.3 to 0.4 s. Here, the suggested method is used to revive Modes B and C in order to reduce grid current imbalance and harmonics. The grid current is disconnected between t = 0.4 and 0.5 s, which causes the controller to enter interruption compensation Mode or Mode D. By using droop control, this mode guarantees a constant supply of load voltage and current. Throughout these intervals, specific voltage and current compensation strategies are employed based on the grid conditions. Figures 5a, 5c, 5e, 5f, and 5d illustrate the responses during each phase, highlighting the series and shunt compensations applied to maintain stable load voltage, mitigate harmonics, and address voltage disturbances effectively. Mode C remains active consistently to handle harmonic compensation caused by nonlinear loads across all operational conditions.

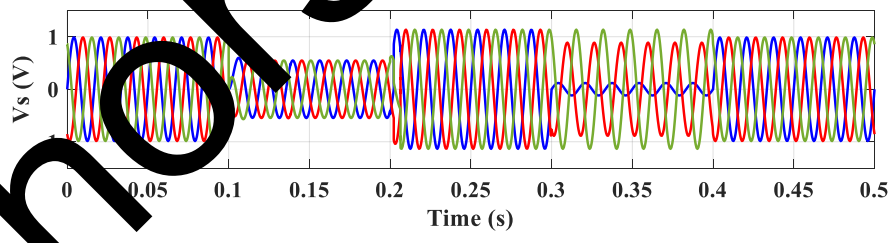

(a)

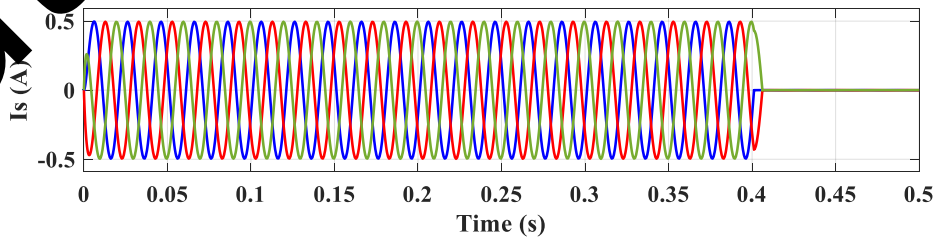

(b)

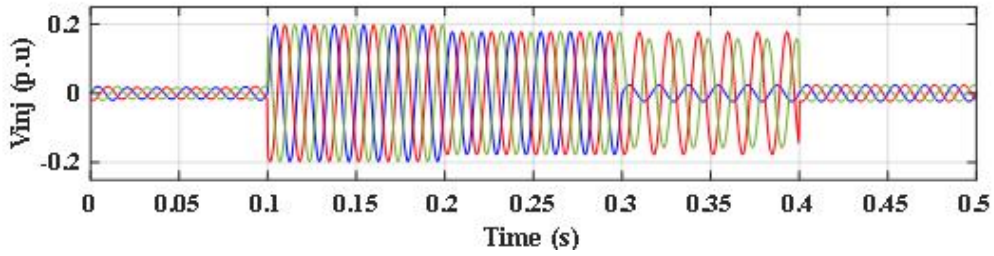

(c)

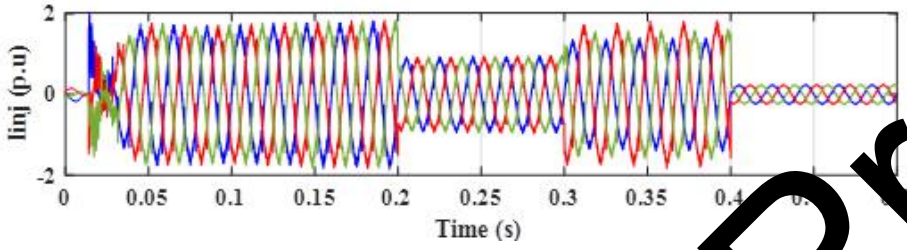

(d)

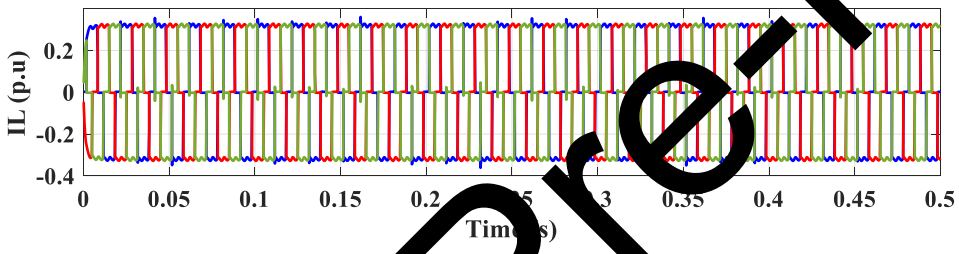

(e)

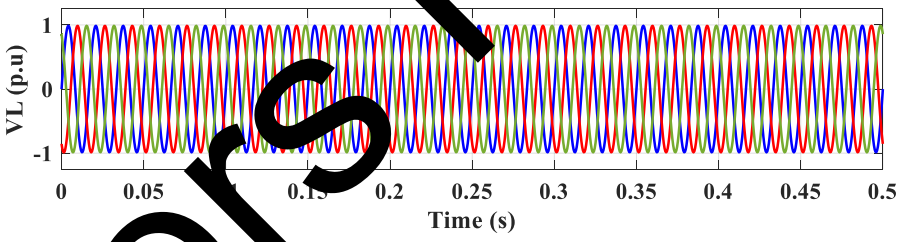

(f)

Figure 5. Analysis of (a) Source voltage, (b) Source current, (c) Series injected voltage (mode B), (d) Shunt injected current (mode C), (e) Nonlinear load current, (f) Load voltage

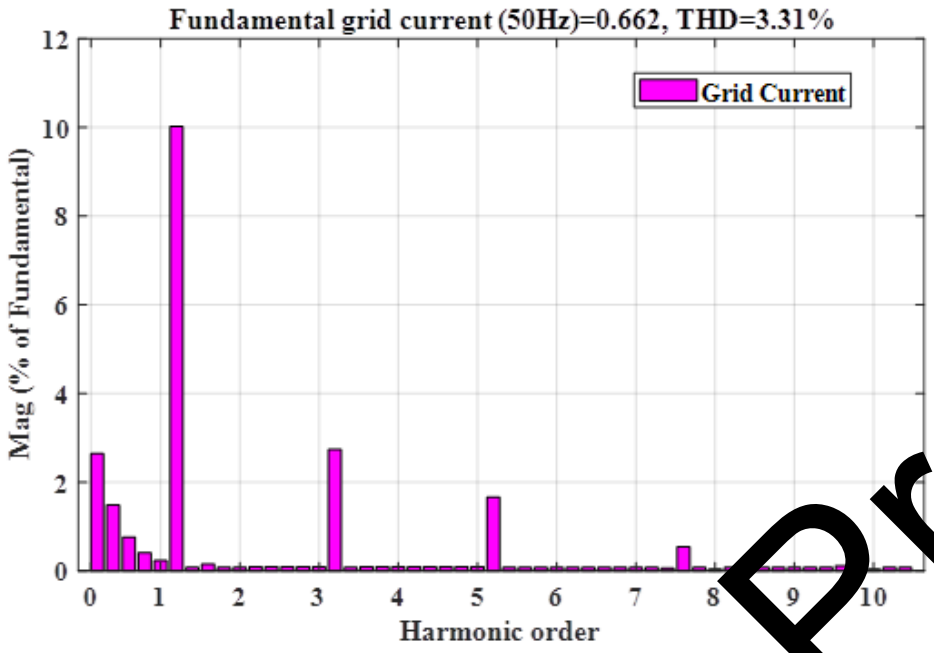

(a)

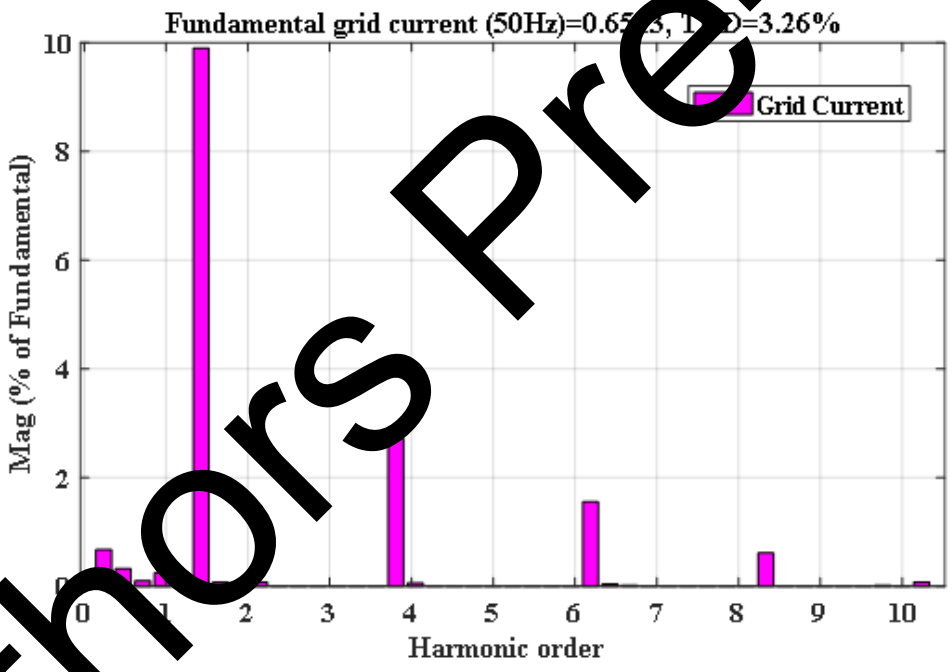

(b)

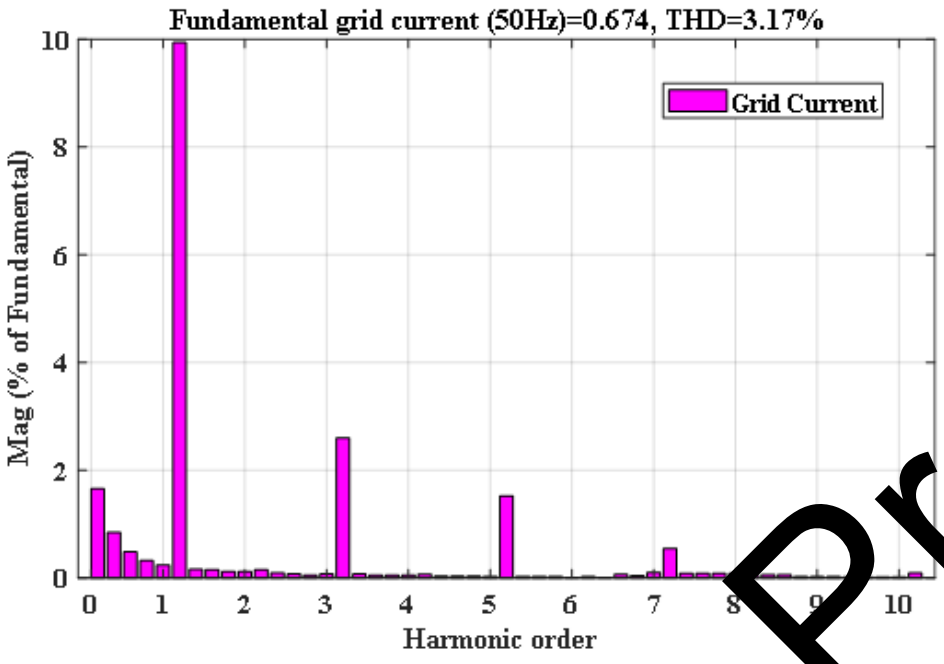

(c)

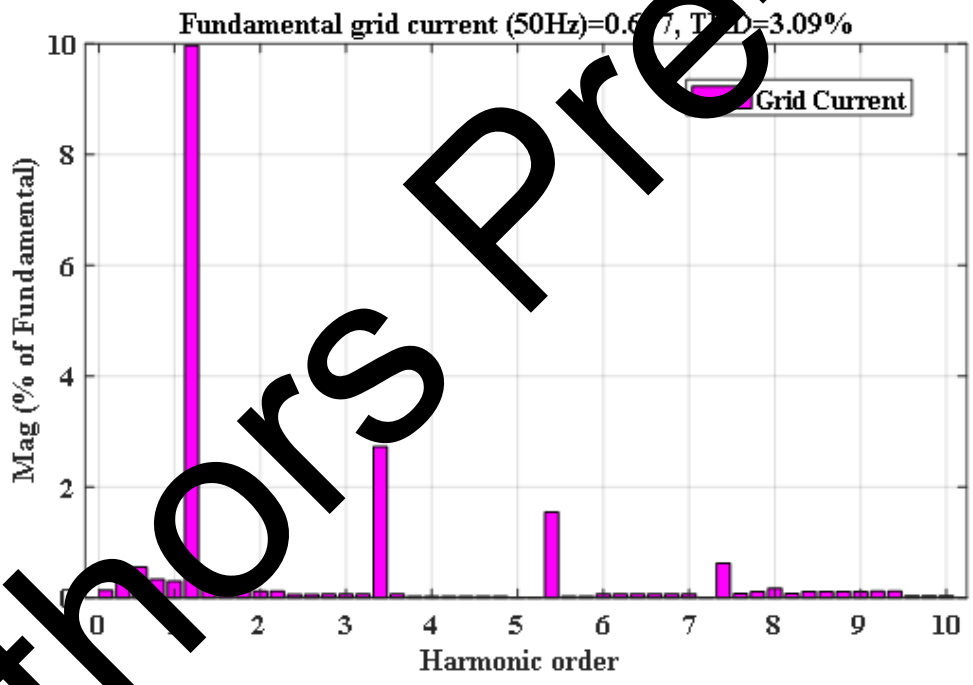

(d)

Figure FFT Evaluation of the grid current (a) 0–0.1s, (b) 0.1s–0.2s, (c) 0.2s–0.3s, (d) 0.3s–0.4s

The grid current Total Harmonic Distortion (THD) exhibits significant reduction across multiple intervals, as demonstrated in Figure 6. The THD of the grid current first drops from 15.09% to 3.73% is given in Figure 6a. Figure 6b illustrates the continuation of this drop, with the THD falling from 15.09% to 3.29%. Referring to Figure 6c, during a subsequent interval, the grid

current THD is decreased from 15.09% to 3.20%. Lastly, Figure 6d displays a drop in the grid current THD to 3.23%. Figure 7 shows the harmonic spectra of the uncompensated grid current and the nonlinear load in the first scenario, emphasizing the spectral content of the load and the grid current prior to the application of compensation techniques.

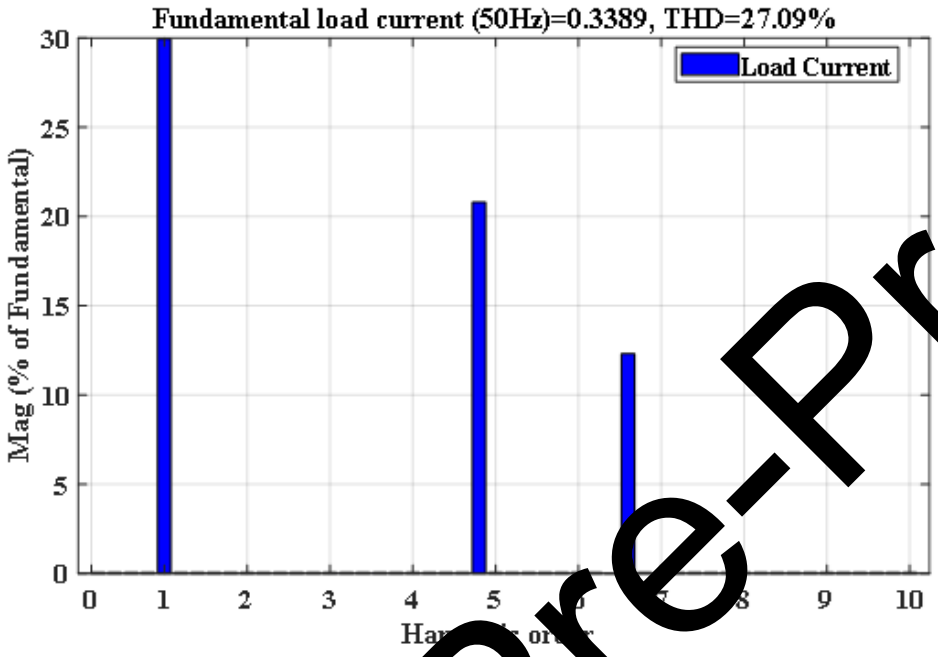

(a)

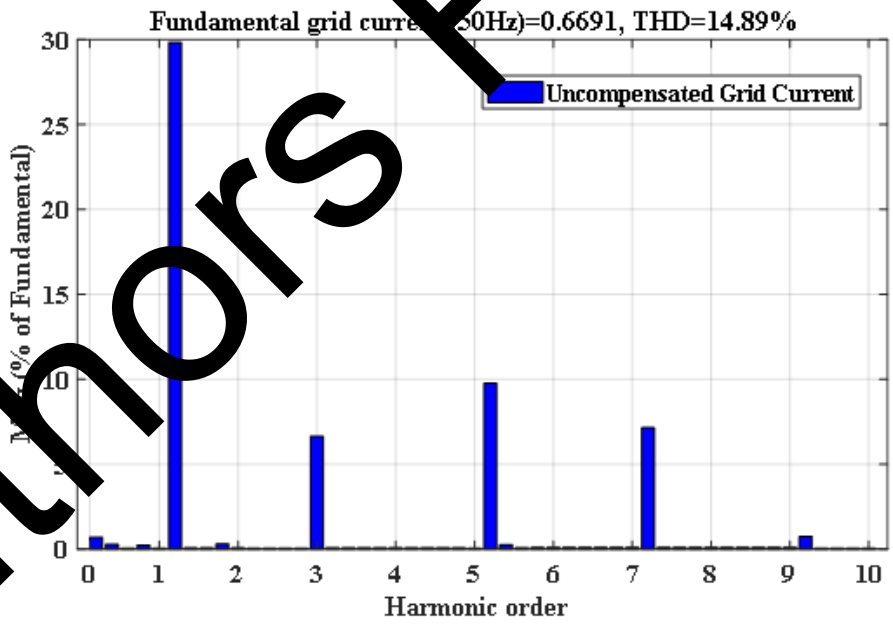

(b)

Figure 7: FFT analysis of (a) nonlinear load and (b) uncompensated grid current in the first case

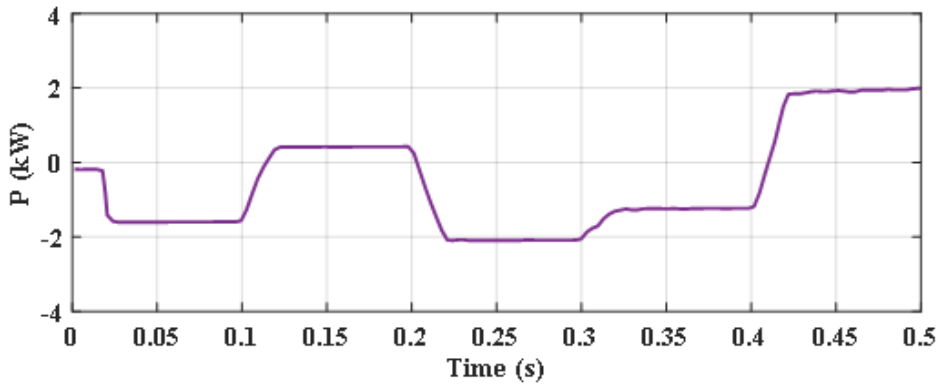

(a)

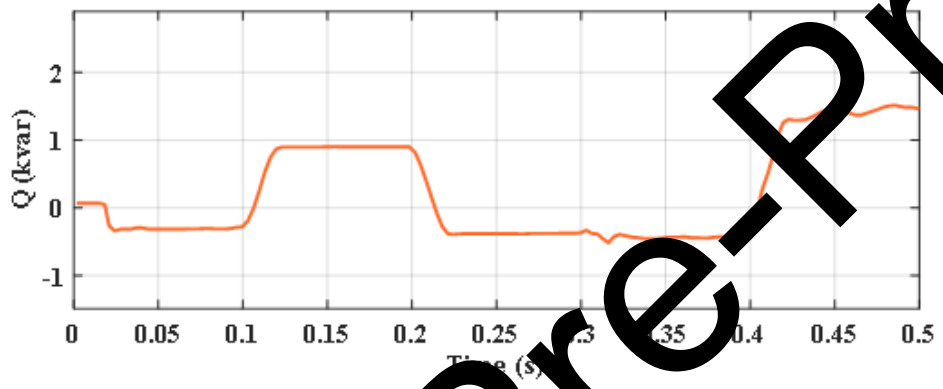

(b)

Figure 8: Analysis of (a) Active power, (b) reactive power

When the nonlinear load is engaged, Figures 8a and 8b show the active and reactive powers that the suggested system exchanges with the grid. The suggested system initially consumes 500 VAR of reactive power and 1 kW of active power between 0 and 0.1s. The system feeds 500 W of active power and 900 VAR of reactive power back to the grid at the interval of 0.1s to 0.2s due to a voltage sag. Next, a voltage swell causes the suggested system to absorb about 500 VAR of reactive power and 1.8 kW of active power between 0.2 and 0.3 seconds. The imbalanced voltage sag causes the system to absorb more active and reactive power in the 0.3–0.4 second time frame. Eventually, the suggested system injects 1.5 kVAR of reactive power and 1.8 kW of active power into the load during the final interval of 0.4 to 0.5 seconds owing to a disruption in the grid currents, proving its ability to stabilise and deliver power during grid disturbances.

(b) Harmonic compensation of load-side due to harmonic source

In these circumstances, the nonlinear load is replaced with a straightforward three-phase resistive load, but the distortion in the source persists. Like in the preceding case, there are simultaneous voltage sags, swells, and interruptions in the source and the grid. The suggested method

successfully keeps the load voltage constant at 1 p.u. in spite of the source-generated disturbances under such difficult operating circumstances. It also makes up for the harmonic components in the load current that exist. Figure 9 presents the simulation results corresponding to scenarios similar to those described in Case (a). The source voltage exhibits significant harmonic distortion, particularly evident in the grid voltages during the time interval from t0 = 0s to t1 = 0.1s, as illustrated in Figure 9a.

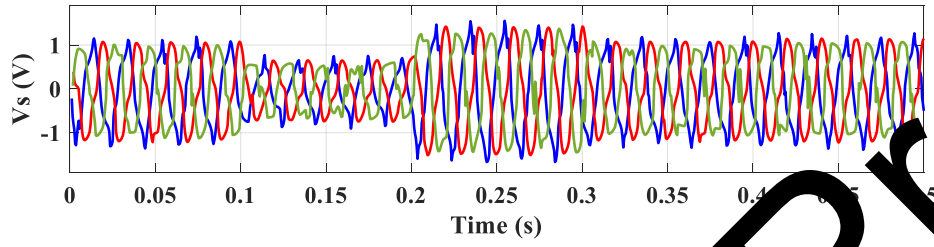

(a)

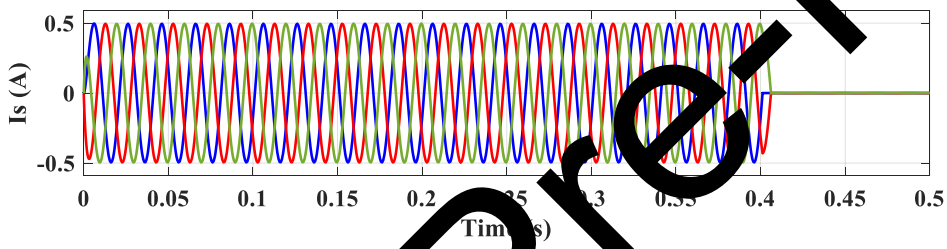

(b)

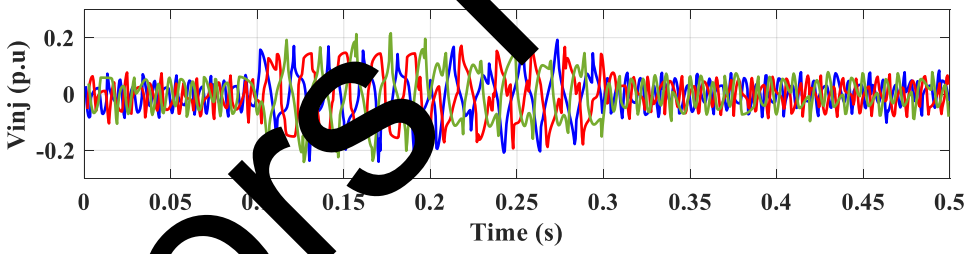

(c)

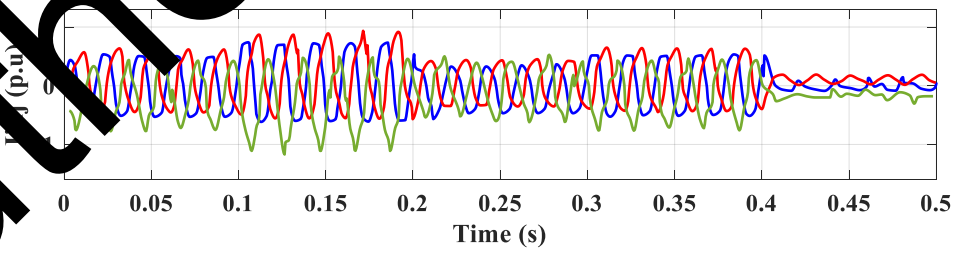

(d)

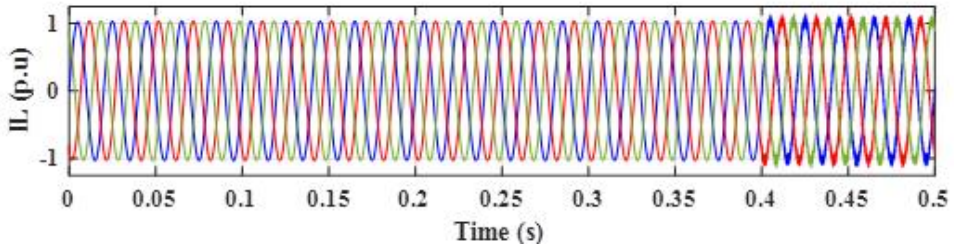

(e)

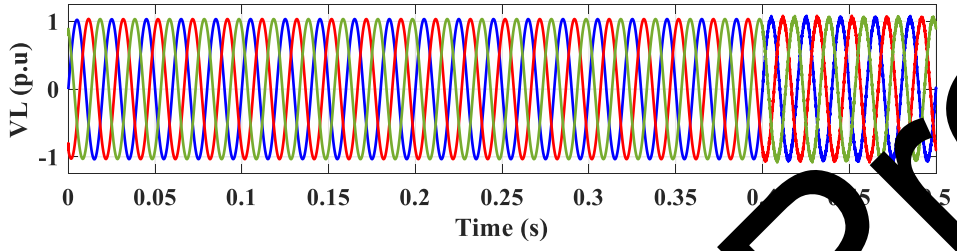

(f)

Figure 9: Analysis of (a) Source voltages, (b) Source currents, (c) Series injected voltages (mode B), (d) Shunt injected currents (mode C), (e) load currents, (f) Load voltages

According to Figure 9b, prior to the interruption at t = 0.4 s, the source currents exhibit balanced magnitudes, despite the presence of distorted grid voltages and currents. The series injected voltage, depicted in Figure 9c, maintains a magnitude of 0.1 p.u. but shows distortion due to the grid voltage harmonics. In Figure 9d, the shunt injected current magnitude is shown to be 0.5 p.u., compensating for the load current harmonics. There is a 0.4 p.u. voltage sag and distortion in the source voltage for the time interval t1 = 0.1s to t2 = 0.2s. As shown in Figure 9c, the suggested approach successfully balances the load voltage in spite of the uneven grid voltage sag. The source voltages continue to be skewed and out of balance as we move forward to t2 = 0.2s to t3 = 0.3s, as seen in Figure 9a. Unbalanced series compensation currents that offset grid voltages are seen in Figure 9c. In order to reduce the load current harmonics, the shunt compensation current, which is depicted in Figure 9d, is also present at a magnitude of 0.4 p.u. In spite of grid current interruption, the suggested approach functions in mode D to supply the linear load from t4 = 0.4s to t5 = 0.5s. As shown in Figures 9e and 9f, this guarantees that voltages and currents remain at 1 p.u. Interestingly, even though the load current THD is 4.5%, it still falls within the allowable limit that IEEE standards have established.

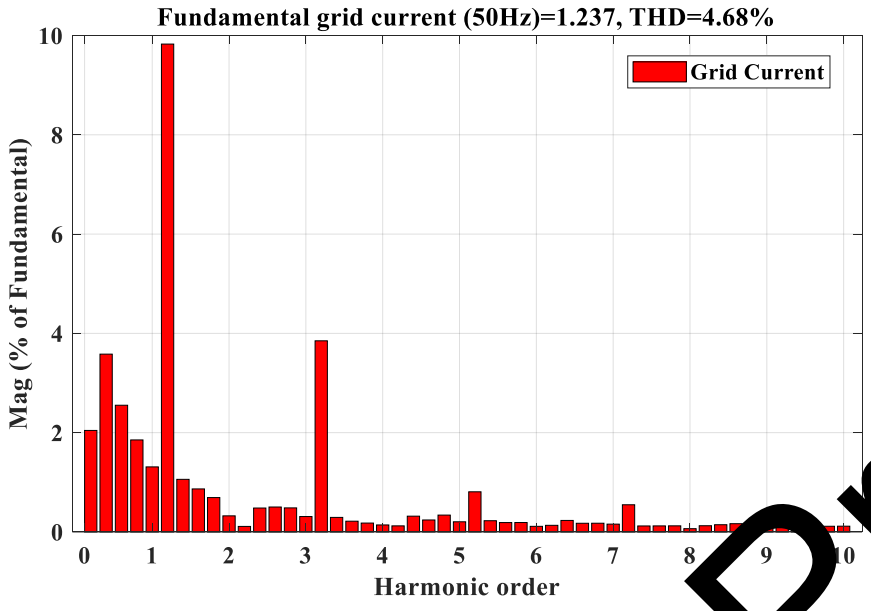

(a)

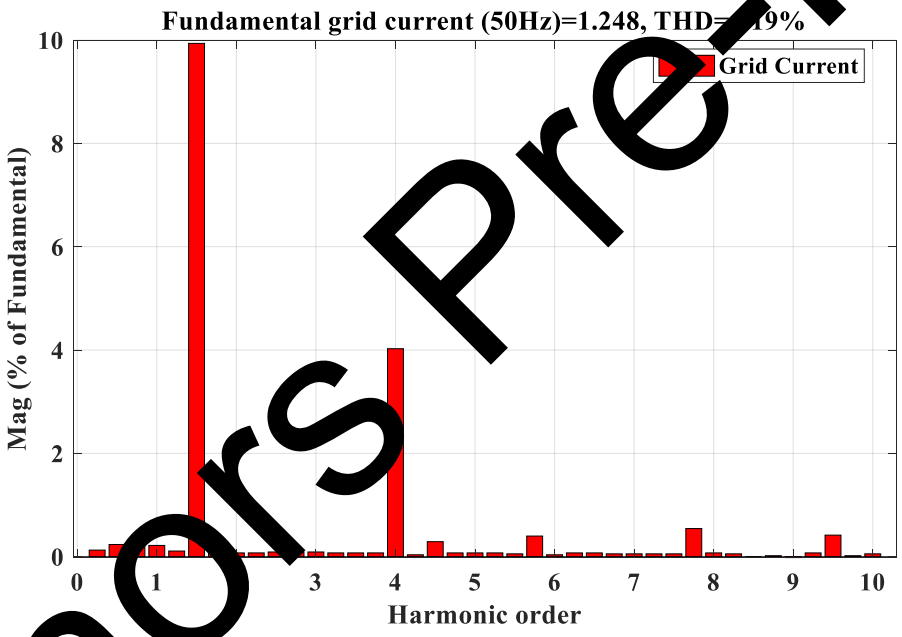

(b)

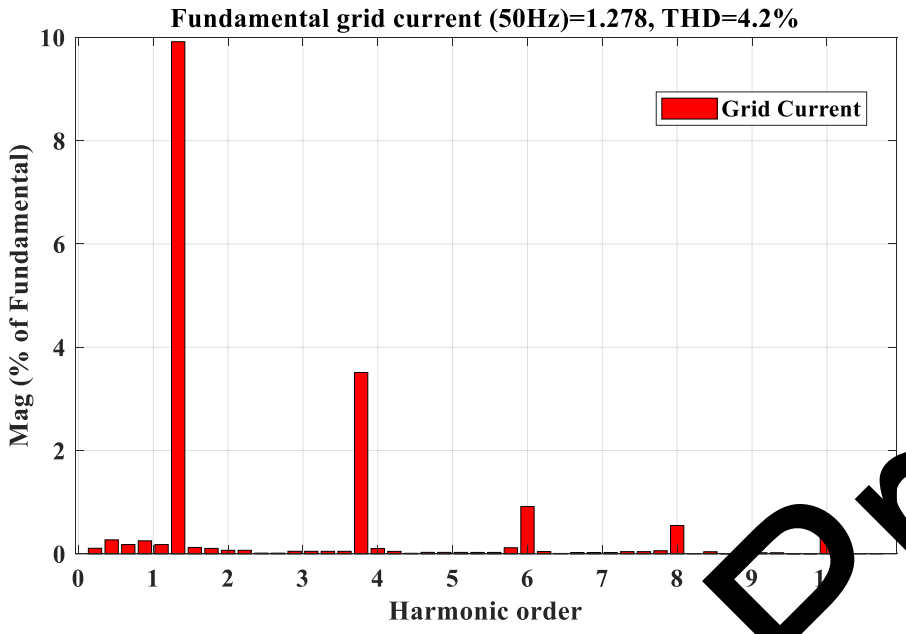

(c)

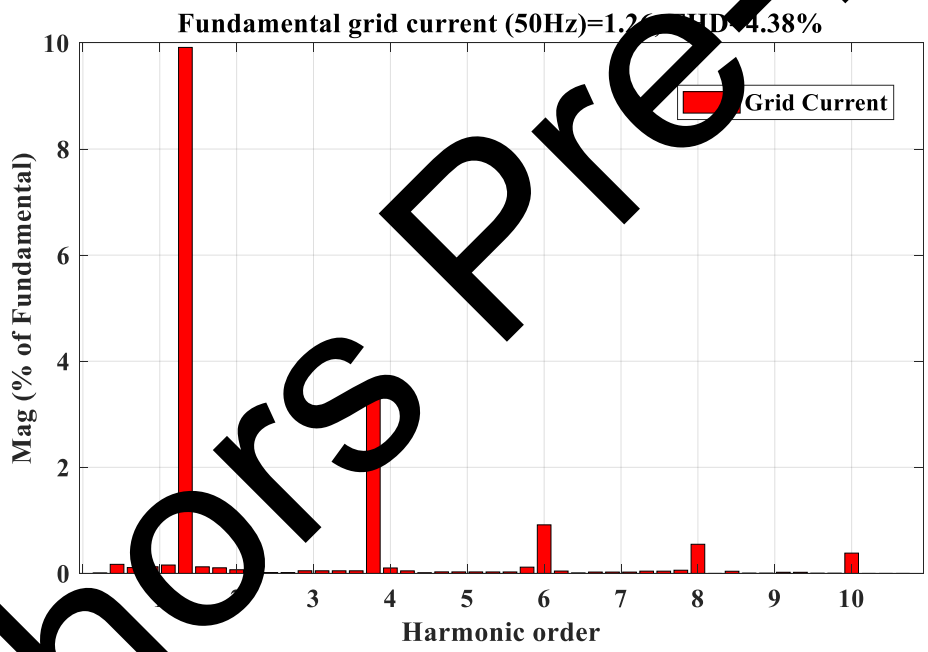

(d)

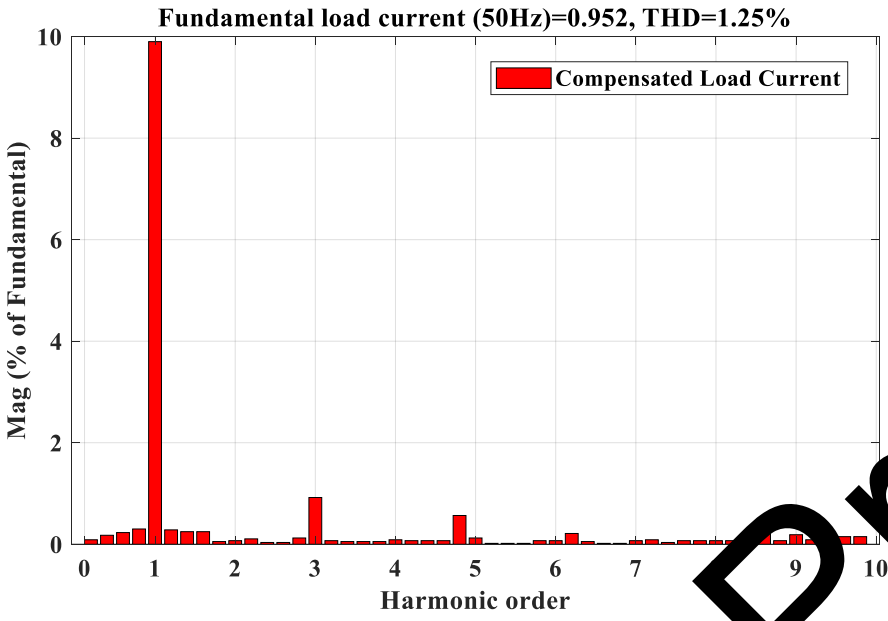

(e)

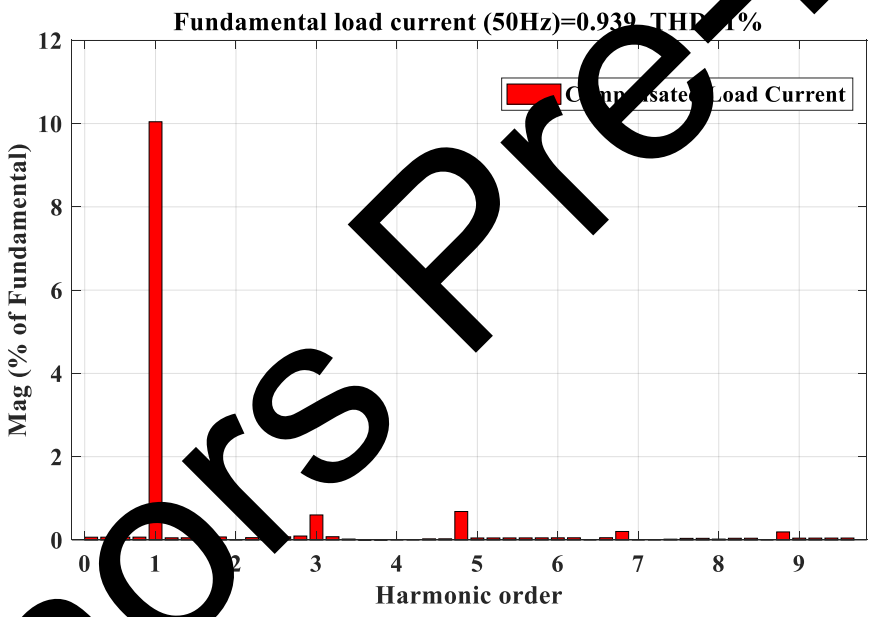

(f)

(g)

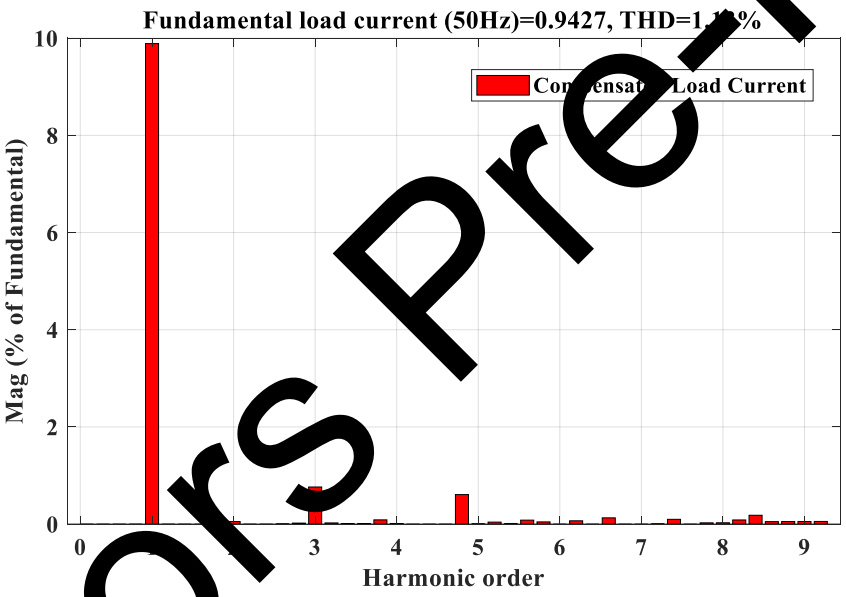

(h)

Figure 10. FFT analysis of (a)–(d) grid current THD, (e)–(h) compensated load current THD

Figure 10a shows a grid current THD of 4.67% for the examined time period. As a result, Figures 10b and 10f show that the grid and load current THDs are, respectively, 4.27% and 1.11%. With a THD of 4.21%, Figure 10c shows that the grid currents are balanced. Furthermore, Figure 10g shows that the load voltages retain a balanced magnitude of 1 p.u. while the currents' THDs measure 0.81%. The conditions between t3 = 0.3s and t4 = 0.4s mirror those of the initial interval and are not further discussed. Moving to Figure 10d, it shows a grid current THD of 4.40%, while concurrently, Figure 10h demonstrates a compensated load current THD of

1.17% during the same interval. These measurements collectively provide insights into the harmonic characteristics and balance of currents and voltages within the specified time frames.

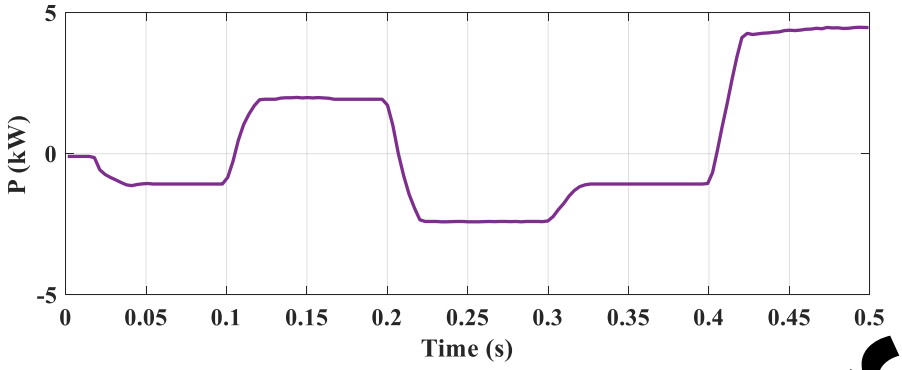

(a)

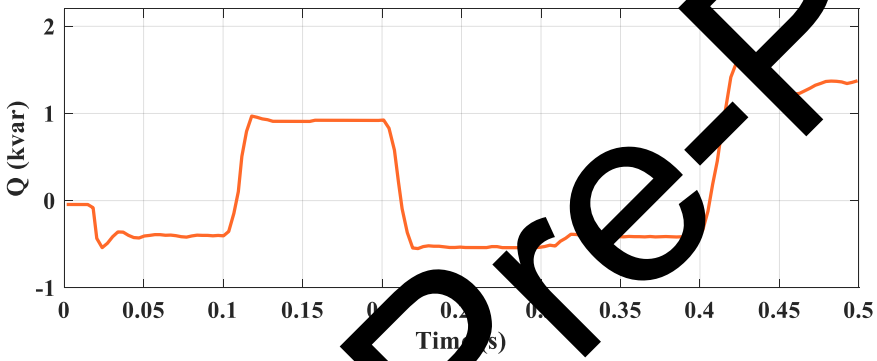

(b)

Figure 11: Evaluation of (a) Active power, (b) reactive power

The suggested system displays variable power absorption and injection characteristics over various time periods, as seen in Figures 11a and 11b. The system consumes 1 kW of active power and 300 VAR of reactive power between 0 and 0.1s. A voltage sag causes the system to feed 2.5 kW of active power and 1 kVAR of reactive power back into the grid as the interval between 0.1 and 0.2 seconds approaches. A voltage swell that occurs between 0.2 and 0.3 seconds requires the system to absorb about 2.5 kW of active power and 500 VAR of reactive power. An unbalanced voltage sag increases the absorption of 1 kW of active power and 200 VAR of reactive power between 0.3 and 0.4 seconds. These fluctuations demonstrate the system's dynamic response to voltage disturbances, ensuring efficient power management and quality maintenance throughout various operational conditions.

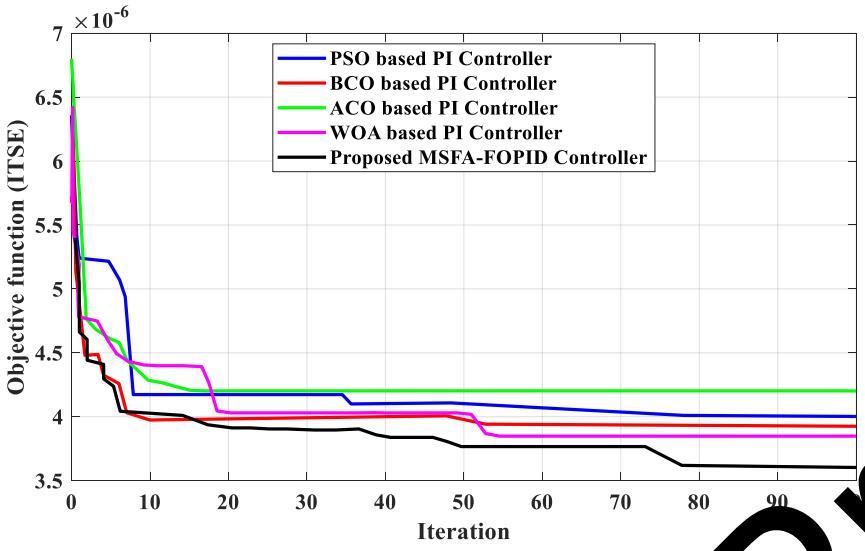

Figure 12: Convergence of ITSE using existing and proposed schemes

The conventional optimization techniques considered in this study include Particle Swarm Optimization (PSO), Bee Colony Optimization (BCO), Ant Colony Optimization, and Whale Optimization Algorithm (WOA). Figure 12 presents the convergence analysis of these optimizers based on the Integral of Time multiplied by Squared Error (ITSE) against iteration count. The plot reveals that the proposed scheme exhibits superior capabilities in both exploitation and exploration. These qualities enable the scheme to effectively optimize controller parameters. Moreover, the average runtime analysis confirms that the proposed scheme achieves faster computation times for solving the objective function compared to the other techniques. In terms of regulating capacitor voltage, the performance of the tuned controllers is evaluated under a 10% step change across the capacitor voltages. This evaluation ensures that the controllers maintain stable and precise regulation of capacitor voltages, validating their effectiveness and robustness in practical applications.

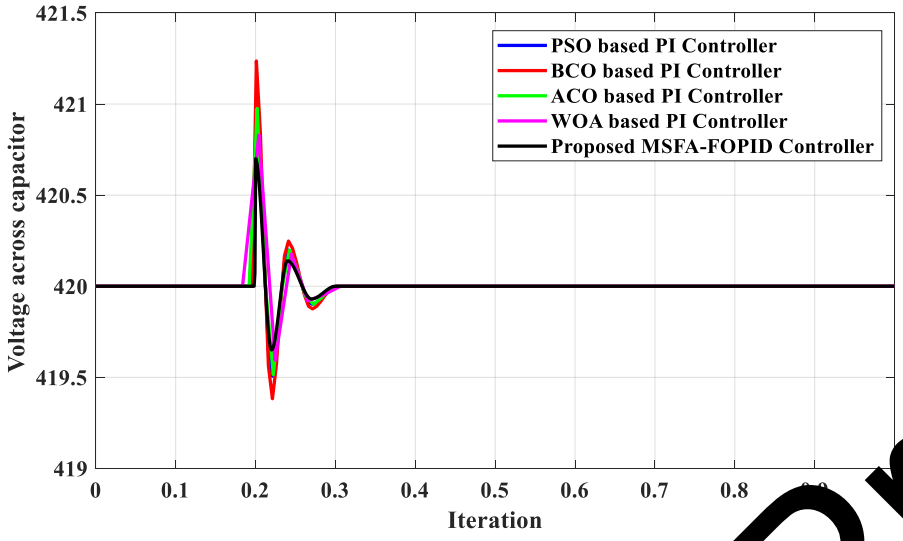

Figure 13: Tuned controller dynamics

The outcomes for the capacitor voltage for each method are depicted in Figure 13. The figure highlights that the proposed controller demonstrates superior dynamics in effectively regulating the voltage across the capacitors.

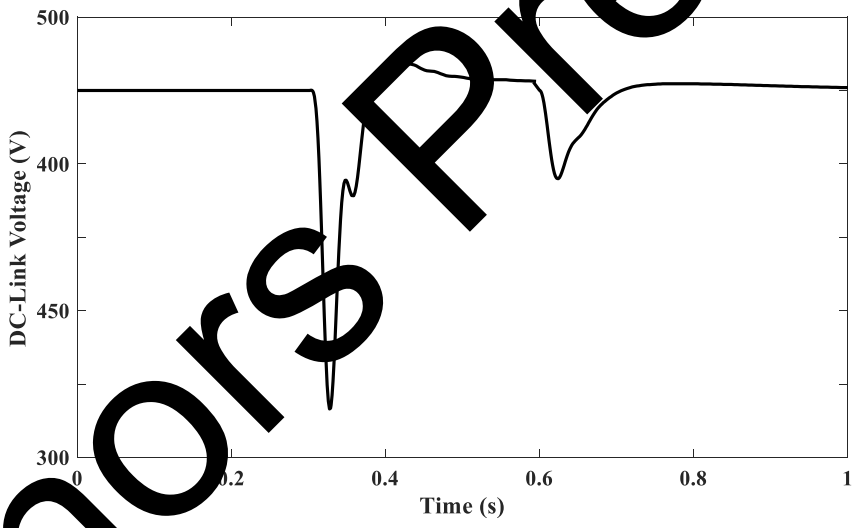

(a)

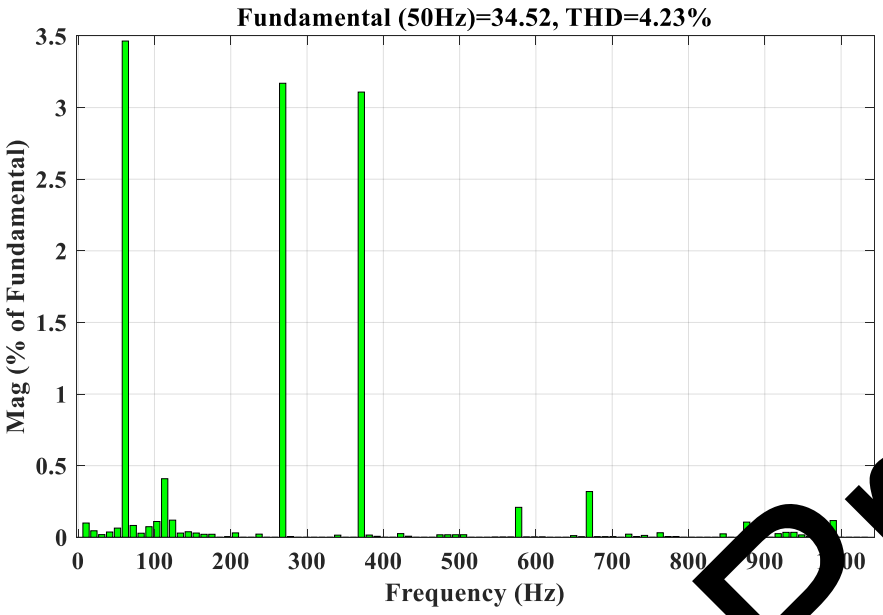

(b)

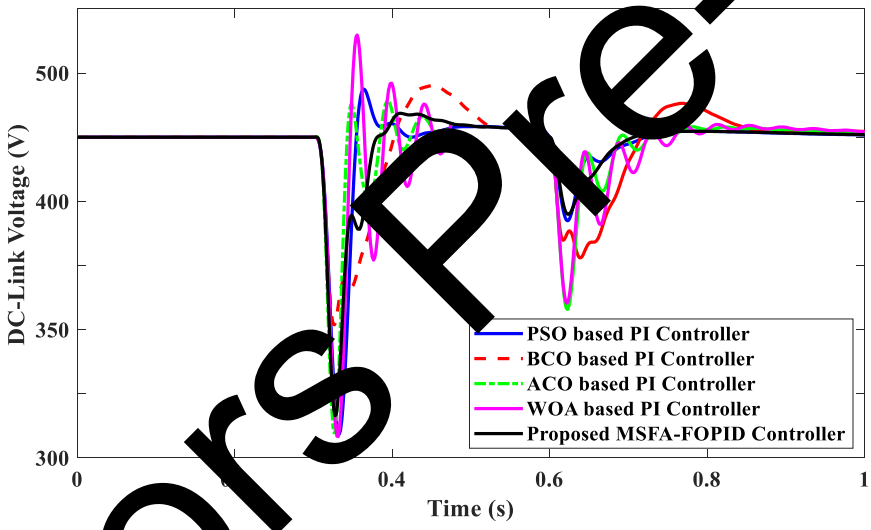

(c)

Figure 14. Behavior of (a) DC-Link Voltage (b) THD analysis in DC link voltage (c) DC link voltage comparison

The voltage across the DC-Link is illustrated in Figure 14a, exhibits sudden oscillations upon connecting the charging system to the grid, attributed to changes in active power flow. However, the voltage stabilizes quickly afterward, underscoring the effectiveness of the designed controller. A comparison of harmonic frequencies before and after compensation is shown in Figure 14b, highlighting the effective suppression achieved by the designed filter. Figure 14c presents the DC-Link voltage dynamics across five designed controllers. Analysis reveals that the proposed controller outperforms others in regulating DC-Link voltage dynamics. This

enhancement also translates into improved HSAF performance, as indicated by the lowest THD observed with the suggested controller compared to alternatives.

Table 1: Statistical summary comparison

			Harmonic pollution (THD in %)			Success rate (%)	Total CPU time (s)
Cases	**Methods**	**Best**	**Worst**	**Mean**	**SD**		
	Proposed controller	0.25	0.37	0.32	0.9	98	150
	WOA based PI	0.28	0.40	0.30	0.11	95	156
Case (a)	**Proposed controller**	0.35	0.44	0.28	0.16	71.3	160.1
	WOA based PI	0.38	0.45	0.25	0.10	68.6	160.3
	ACO based PI	0.35	0.48	0.23	0.17	65.7	167.5
	BCO based PI	0.37	0.49	0.25	0.20	63.4	168.3
	PSO based PI	0.39	0.50	0.24	0.24	66.8	168.6
Case (b)	**Proposed controller**	0.20	0.23	0.3	0.19	96.4	154.2
	WOA based PI	0.21	0.24	0.30	0.20	80.5	156.8
	ACO based PI	0.22	0.26	0.28	0.26	81.2	163.5
	BCO based PI	0.2	0.30	0.27	0.29	82	165.6
	PSO based PI	0.23	0.34	0.27	0.30	83.3	167

Table 2: Comparison of THD (%)

Case	Techniques	THD (%) at different load ratings				
		10Ω	**20Ω**	**30Ω**	**40Ω**	**50Ω**
	PSO based PI	13.57	13.57	13.57	13.57	13.57
	BCO based PI	11.74	11.73	11.72	11.70	11.67
	ACO based PI	12.65	13.65	13.76	14.76	12.21

	WOA based PI	13.64	15.74	17.67	15.64	13.63
	Proposed controller	13.95	14.67	14.56	15.87	16.67
Case (a)	**GOA**	14.65	14.88	15.86	16.76	17.74
	PI	15	15.14	16.27	15.04	12.13
	PSO based PI	14.64	15.45	18.54	16.14	15.2
	BCO based PI	19.30	19.50	28.56	[illegible]	[illegible]
	ACO based PI	20.45	21.65	29.76	[illegible]	15.76
	WOA based PI	21.34	24.45	[illegible]	13.78	16.52
	Proposed controller	22.35	27	[illegible]	13	17.86
Case (b)	**PSO based PI**	22.75	[illegible]	33.56	13.98	19
	BCO based PI	26	[illegible]	36.55	14	17.33
	ACO based PI	[illegible]	31	36.78	14.87	17
	WOA based PI	21.53	18	27.56	9.86	24
	Proposed controller	21.87	19.76	28	11.65	25.76

Table 1 presents a statistical examination of six case studies that employ various techniques along with the Hybrid Shunt Active Filter (HSAF) setup to assess how well the proposed approach works. This table compiles the optimal THD percentage, poorest THD percentage, average THD, standard deviation, success percentage, and processing time achieved through the recommended technique. These statistical findings are measured against existing approaches to identify superior performance. Additionally, Table 2 displays a comparison of THD (%)

measurements across different load capacities (10Ω, 20Ω, 30Ω, 40Ω, and 50Ω) both with and without the control system. The combined findings from Tables 1 and 2 demonstrate that the recommended approach incorporating PV integration outperforms other control methods, evidenced by its reduced THD percentages.

4.1. Discussions

The research results shown offer important consequences for power electronics and control system fields. First, the proposed controller's proven ability to manage DC-Link voltage during unexpected fluctuations caused by changing active power flows highlights its durability and fitness for practical use. This steadiness directly helps boost the dependability and performance of grid-connected power systems, especially when handling temporary disturbances.

Additionally, comparing harmonic frequencies both before and after compensation, as displayed in the harmonic evaluation, shows that the created filter successfully reduces harmonics, thus improving total power quality. This element is essential for meeting strict regulatory requirements and guaranteeing seamless functioning of delicate electronic devices.

The noted exceptional performance of the suggested controller in lowering THD demonstrates its ability to improve HSAF performance. This approach not only cuts down operating expenses related to harmonic distortions but also extends the service life of attached equipment. Research results reveal a promise of sophisticated optimization methods like those suggested in boosting power system stability, performance, and quality. This paves away for future progress in smart grid technology and environmentally safe energy solutions.

5. Conclusions

This research employs the MATLAB/Simulink environment to develop a proposed control method for eliminating harmonics in multilevel inverters. The control approach utilizes a Hybrid Shunt Active Filter (HSAF) to accurately deliver compensation currents when harmonic distortion occurs, aiming to enhance PV power extraction efficiency. Performance evaluation of the proposed control technique relies on THD percentage measurements. The strategy's effectiveness is determined by comparing its results against other control methodologies. Simulation findings demonstrate that the proposed approach outperforms existing methods, achieving reduced THD levels across different loading conditions. The simulation study outcomes reveal that the proposed method for multilevel inverter harmonic mitigation proves highly effective. The calibrated controllers undergo testing to evaluate their capacity for capacitor voltage regulation when exposed to a 10% step variation across the capacitors. The

optimization structure should be expanded to encompass multiple goals including loss reduction, power factor enhancement, and system efficiency improvement alongside harmonic suppression. Multi-objective optimization offers a comprehensive solution that addresses competing requirements.

References

[1] T. Lee, Y. Wang, J. Li and J. Guerrero, "Hybrid Active Filter With Variable Conductance for Harmonic Resonance Suppression in Industrial Power Systems", IEEE Transactions on Industrial Electronics, vol. 62, no. 2, pp. 746-756, 2015.

[2] Terciyanli, T. Avci, İ. Yilmaz, C. Ermis, K. Kose, A. Acik, A. Kalaycioglu, Y. Akkaya, I. Cadirci and M. Eris, "A Current Source Converter-Based Active Power Filter for Mitigation of Harmonics at the Interface of Distribution and Transmission Systems", IEEE Transactions on Industry Applications, vol. 48, no. 4, pp. 1374-1386, 2012.

[3] S. Mikkili and A. Panda, "Simulation and real-time implementation of shunt active filter id–iq control strategy for mitigation of harmonics with different fuzzy membership functions", IET Power Electronics, vol. 5, no. 9, pp. 1856-1870, 2012.

[4] Panda and S. Mikkili, "FLC based shunt active filter (p–q and Id–Iq) control strategies for mitigation of harmonics with different fuzzy MFs using MATLAB and real-time digital simulator", International Journal of Electrical Power & Energy Systems, vol. 47, pp. 313-336, 2013.

[5] R. Patel and A. Panda, "Real-time implementation of PI and fuzzy logic controller based 3-phase 4-wire interleaved buck active power filter for mitigation of harmonics with id–iq control strategy", International Journal of Electrical Power & Energy Systems, vol. 59, pp. 66-78, 2014.

[6] Micallef, M. Apap, C. Spiteri-Staines and J. Guerrero, "Mitigation of Harmonics in Grid-Connected and Islanded Microgrids Via Virtual Admittances and Impedances", IEEE Transactions on Smart Grid, pp. 1-11, 2015.

[7] M. Zavvari and A. Chudasama, "Control strategies for harmonic mitigation and power factor correction using shunt active filter under various source voltage conditions", International Journal of Electrical Power & Energy Systems, vol. 42, no. 1, pp. 661-671, 2012.

[8] Marzoughi, H. Imaneini and A. Moeini, "An optimal selective harmonic mitigation technique for high power converters", International Journal of Electrical Power & Energy Systems, vol. 49, pp. 34-39, 2013.

[9] T. Zaveri, B. Bhalja and N. Zaveri, "Comparison of control strategies for DSTATCOM in three-phase, four-wire distribution system for power quality improvement under various source voltage and load conditions", International Journal of Electrical Power & Energy Systems, vol. 43, no. 1, pp. 582-594, 2012.

[10] M. Barghi Latran, Y. Yoldaş and A. Teke, "Mitigation of power quality problems using distribution static synchronous compensator: a comprehensive review", IET Power Electronics, vol. 8, no. 7, pp. 1312-1328, 2015.

[11] Reguieg, Z., Bouyakoub, I. and Mehedi, F., 2024. Optimizing power quality in interconnected renewable energy systems: series active power filter integration for harmonic reduction and enhanced performance. Electrical Engineering, pp.1-14.

[12] Mukherjee, S., Mandal, R. and Chatterjee, S., 2024. Comparison of Harmonic Mitigation Techniques for Grid-Connected PV System and Introduction of a Concept of Hybrid Filter. Applied Solar Energy, 60(1), pp.138-148.

[13] Nor, K.A.M. and Abdullah, N., 2024. Power quality improvement of three-phase electrical systems using active-passive hybrid harmonic filter. Results in Engineering, 22, p.102242.

[14] Li, S., Wu, J., Vasquez, J.C., Guerrero, J.M., Pavlinsky, A. and Lekić, A., 2024. Active filter parameter tuning method for harmonic voltage mitigation in wind power plants. Electric Power Systems Research, 234, p.110706.

[15] Amini, B., Rastegar, H. and Pichan, M., 2024. An optimized proportional resonant current controller based genetic algorithm for enhancing shunt active power filter performance. International Journal of Electrical Power & Energy Systems, 156, p.109738.

[16] Govind, A., Jayaswal, K., Tayal, V.K. and Kumar, P., 2024. Simulation and real time implementation of shunt active power filter for power quality enhancement using adaptive neural network topology. Electric Power Systems Research, 228, p.110042.

[17] Rezapour, H., Mathnia, F., Fiuzy, M., Falaghi, H. and Lopes, A.M., 2024. Enhancing power quality and loss optimization in distorted distribution networks utilizing capacitors and active power filters: A simultaneous approach. International Journal of Electrical Power & Energy Systems, 155, p.109590.

[18] Karbasforooshan, M.S. and Monfared, M., 2024. Grid voltage sensorless control of a single-phase shunt hybrid active power filter. IET Power Electronics, 17(6), pp.752-763.

[19] Daramukkala, P., Mohanty, K.B. and Behera, B.P., 2024. Improved performance of a shunt hybrid active power filter by a robust exponential functional link network-based nonlinear adaptive filter control to enhance power quality. ISA transactions.

[20] Gupta, U.K., Sethi, D. and Goswami, P.K., 2024. Adaptive TS-ANFIS neuro-fuzzy controller based single phase shunt active power filter to mitigate sensitive power quality issues in IoT devices. e-Prime-Advances in Electrical Engineering, Electronics and Energy, 8, p.100542.

[21] Wang, Y., Xu, J., Feng, L. and Wang, C., 2017. A novel hybrid modular three-level shunt active power filter. IEEE Transactions on Power Electronics, 33(9), pp.7591-7600.

[22] Tepljakov, A., Alagoz, B.B., Yeroglu, C., Gonzalez, E., HosseinNia, S.H. and Petlenkov, E., 2018. FOPID controllers and their industrial applications: A survey of recent results. IFAC-PapersOnLine, 51(4), pp.25-30.

[23] Du, W. and Li, B., 2008. Multi-strategy ensemble particle swarm optimization for dynamic optimization. Information sciences, 178(15), pp.3096-3109.

[24] Trojovská, E., Dehghani, M. and Trojovský, P., 2022. Fennec fox optimization: A new nature-inspired optimization algorithm. IEEE Access, 10, pp.84417-84443.